Approximate peak time to time-domain fluorescence diffuse optical tomography for nonzero fluorescence lifetime

Shuli Chen, Junyong Eom*, Gen Nakamura, Goro Nishimura

November 26, 2024

Abstract

This paper concerns an inverse problem for fluorescence diffuse optical tomography (FDOT) reconstructing locations of multiple point targets from the measured temporal response functions. The targets are multiple fluorescent point objects with a nonzero fluorescence lifetime at unknown locations. Peak time, when the temporal response function of the fluorescence reaches its maximum, is a robust parameter of the temporal response function in FDOT because it is most less suffered by the artifacts, such as noise, and is easily determined by experiments. We derive an approximate peak time equation based on asymptotic analysis in an explicit way in the case of nonzero fluorescence lifetime when there are single and multiple point targets. The performance of the approximation is numerically verified. Then, we develop a bisection algorithm to reconstruct the location of a single point target from the algorithm proposed in [4] for the case of zero fluorescence lifetime. Moreover, we propose a boundary-scan algorithm for the reconstruction of locations of multiple point targets. Finally, several numerical experiments are implemented to show the efficiency and robustness of the addressed algorithms.

Keywords. FDOT, Asymptotic analysis, Peak time, Reconstruction algorithm.

MSC(2010): 35R30, 35K20.

Addresses:

S. Chen: School of Mathematics, Southeast University, Nanjing 210096, P. R. China.
E-mail: `sli_chen@126.com`   ORCID ID: 0009-0000-6563-5312

J. Eom: Research Institute for Electronic Science, Hokkaido University, Sapporo 001-0020, Japan.
E-mail: `eom@es.hokudai.ac.jp`   ORCID ID: 0000-0002-2749-3322

G. Nakamura: Department of Mathematics, Hokkaido University, Sapporo 060-0810, Research Institute for Electronic Science, Hokkaido University, Sapporo 001-0020, Japan.
E-mail: `nakamuragenn@gmail.com`   ORCID ID: 0000-0002-7911-8612

G. Nishimura: Research Institute for Electronic Science, Hokkaido University, Sapporo 001-0020, Japan.
E-mail: `gnishi@es.hokudai.ac.jp`   ORCID ID: 0000-0003-4330-2626

---

*Corresponding author

1 Introduction

Fluorescence diffuse optical tomography (FDOT) is one of the imaging techniques using fluorescence light from fluorophores in highly scattering media. In particular, this technique is essential in biological or medical applications for tissues *in vivo* to visualize specific diseases and biological activities using fluorescent probes by reconstructing their unknown regions from the measurements outside tissue [17, 19, 20]. Although the importance of imaging inside tissue is well understood, the problems caused by the highly scattering media do not allow using standard imaging techniques, requiring a special imaging technique, FDOT. This imaging technique is also called fluorescence molecular tomography (FMT) and is categorized as a kind of diffuse optical tomography (DOT) using fluorescence. In highly scattering media like biological tissue, the light path is not straight anymore, and the repeating scattering makes the light propagation an energy dissipation process approximately described by a diffusion equation. Eventually, a reconstruction method based on the light propagation model is required to visualize the three-dimensional fluorescence distribution, recovering the quantitative information by measurements on the boundary of the medium [12, 13]. The FDOT is categorized by the measurement data types [9, 11], such as the steady-state fluorescence intensity (CW method)[3, 8], the temporal response function of the fluorescence intensity (time-domain method)[15, 23], the phase and demodulation of the fluorescence intensity (frequency-domain method)[1, 18] and a hybrid method of them [22]. We choose the time-domain method because the temporal response function has direct information on the distribution of optical paths determined by the geometry, the position of the injection point of the excitation light, the distribution of the fluorophores, and the detection point of the fluorescence.

In this paper, we analyze the temporal response function. The measured temporal response function is a set of the intensities of detected light in a certain time period at certain times after the instantaneous light injection like a delta function, and the time reflects the optical path length of a trajectory in the medium [10], and it delays, in our case, by the staying time at the excited state of fluorophore determined by the fluorescence lifetime. Namely, the measured temporal response function is a discretized temporal response function, which is given by the solution of the light propagation model and reflects the optical path length distribution function associated with the target location. Then, we focus on the peak time, which will be defined as the time when the function becomes maximum, to characterize the temporal response function for the inputs of the reconstruction of targets. The maximum position of the temporal response function is least affected by the noises and artifacts due to environmental contamination and should be robustly determined. In addition, the peak position reflects the most likely optical path length for the light in the variety of travels from the source to the detector, which is determined by the distances between the source, the target, and the detector.

Next, we start to formulate our inverse problem. We first consider the measurements of the fluorescence targets in tissue like the human chest, which is considerably larger than the measurable distances, resulting in the boundary being an approximately infinite plane. Thus, we consider a medium $\Omega := \mathbb{R}^3_+$ with boundary $\partial\Omega$. Let u_e and U_m be excitation and emission light for the fluorescence process, respectively. These two processes can be modeled as the following coupled diffusion equations [16]:

$$\begin{cases} \left(v^{-1}\partial_t - D\Delta + \mu_a\right) u_e = 0, & (x,t) \in \Omega \times (0,\infty), \\ u_e = 0, & (x,t) \in \bar{\Omega} \times \{0\}, \\ \partial_\nu u_e + \beta u_e = \delta\left(x - x_s\right)\delta(t), & (x,t) \in \partial\Omega \times (0,\infty) \end{cases} \tag{1.1}$$

and

$$\begin{cases} \left(v^{-1}\partial_t - D\Delta + \mu_a\right) U_m = \mu(f_\ell * u_e), & (x,t) \in \Omega \times (0,\infty), \\ U_m = 0, & (x,t) \in \bar{\Omega} \times \{0\}, \\ \partial_\nu U_m + \beta U_m = 0, & (x,t) \in \partial\Omega \times (0,\infty). \end{cases} \tag{1.2}$$

Here, $\partial_\nu := \nu \cdot \nabla$ is the exterior normal derivative, v is the speed of light in the medium, D is the diffusion constant, μ_a is the absorption coefficient, and $\beta = b/D > 0$ is a positive constant coming from the Fresnel reflection at the boundary, $b \in [0,1]$, due to the refractive index mismatch at the boundary. Also, $\delta(\cdot)$ denotes

the delta function, and $x_s \in \partial\Omega$ is the position of the point source where the excitation light is injected. Further, the source term, which corresponds to the fluorescence emission from the fluorophores, for U_m on the right-hand side of (1.2) is given as

$$\mu(f_\ell * u_e)(x, t) := \mu(x) \int_0^t \ell^{-1} e^{-\frac{t-s}{\ell}} u_e(x, s; x_s) \, ds, \tag{1.3}$$

where $\mu(x) > 0$ is the absorption coefficient of a fluorophore, and $f_\ell * u_e$ is the convolution of u_e and the fluorescence decay function, $f_\ell(t) := \ell^{-1} e^{-t/\ell}$, $t \geq 0$, with the fluorescence lifetime $\ell > 0$. Note that if $\ell \to 0$, it is easy to see that $\mu(f_\ell * u_e)(x, t) = \mu(x) u_e(x, t; x_s)$. Hence, we extend the definition of (1.3) to the case that the zero fluorescence lifetime ($\ell = 0$) by defining its right-hand side by $\mu(x) u_e(x, t; x_s)$.

Then, our inverse problem is formulated as follows.

Inverse Problem: Let

$$\mu(x) = \sum_{j=1}^J c_j \delta(x - x_c^{(j)}), \tag{1.4}$$

where each $x_c^{(j)}$ is the location of j-th unknown target, and each unknown c_j is the absorption strength committed fluorescence by the target at $x_c^{(j)}$. Then, reconstruct each $x_c^{(j)}$ from the measured peak times given as

$$t_{peak}^{(n)} := t_{peak}(x_d^{(n)}, x_s^{(n)}) = \arg\max_{t>0} U_m(x_d^{(n)}, t; x_s^{(n)}), \; n = 1, 2, \cdots, N,$$

where $\left\{ \{x_d^{(n)}, x_s^{(n)}\} \right\}_{n=1}^N$ are N sets of S-D pairs consisting of detector points $\{x_d^{(n)}\}_{n=1}^N$ and source points $\{x_s^{(n)}\}_{n=1}^N$ located on $\partial\Omega$. For $J = 1$ and $J \geq 2$, we call μ single point target and multiple point targets, respectively.

Now, we briefly review some related works to the mentioned inverse problem in historical order, where the peak time of the time-domain data is studied or further used to solve the inverse problem. In [6, 7], the authors considered the case of $\ell > 0$ and $\beta = 0$. They reconstructed the depth of the point target by numerically calculating the peak time without giving any of the formulas derived in a mathematically rigorous way. Then in [5], the authors considered the case of $\ell = 0$. By using the asymptotic analysis for the formula of the solution to (1.2), they derived explicit expressions of the approximate peak time equations for the cases $\beta = 0$, $\beta > 0$, and $\beta = \infty$ in (1.1) and (1.2). Further, in [4], the authors of this paper gave a better expression for the asymptotic behavior of the mentioned solution for the case $\ell = 0, \beta > 0$ and derived an approximate peak time equation. Also, this equation led them to propose a bisection reconstruction algorithm to reconstruct the location of the point target and verify its accuracy and robustness.

We provide an asymptotic behavior of the solution U_m to (1.2) and derive an approximate peak time equation in the case of nonzero fluorescence lifetime, $\ell > 0$. Since the effect from the fluorescence decay function f_ℓ in (1.3) is not negligible in the practical range of $\ell > 0$, resulting in a clear difference in the peak times between zero lifetime solution and nonzero fluorescence lifetime solution U_m, we consider the case $\ell \gg 1$, i.e. large enough fluorescence lifetime. Then, the asymptotic behavior of the solution U_m is written in terms of the integral (See (2.2))

$$\int_0^t u_m(s) \, ds,$$

where u_m is the solution to (1.2) with zero fluorescence lifetime $\ell = 0$. We can approximate the above integral by replacing u_m as u_m^a, where u_m^a is the asymptotic profile of u_m when the depth of the point target is large enough (See Lemma 2.1). In Theorem 2.3, we provide the asymptotic behavior for

$$\int_0^t u_m^a(s) \, ds \sim k^{-\frac{3}{4}} (\pi\lambda)^{\frac{1}{2}} u_m^a(\lambda k^{-\frac{1}{2}}), \; \lambda \gg 1 \quad \text{with} \quad k := \mu_a v, \quad \lambda^2 := \frac{|x_d - x_c|^2 + |x_s - x_c|^2}{2vD}, \tag{1.5}$$

3

which enables us to derive the asymptotic behavior for the solution U_m to (1.2) and define approximate peak time $t > 0$ as a solution of

$$\lambda e^{-\frac{(\sqrt{k}t-\lambda)^2}{t}} = \pi^{\frac{1}{2}} \ell^{-1} t^{\frac{3}{2}}. \tag{1.6}$$

Here, we note that $\lambda > 0$ is an important parameter, which is a constant times the square root of the sum of two squares of distances which are the distances from the target x_c to the detector x_d and the source x_s.

The advantage of the proposed approximate peak time equation (1.6) is that it has an explicit and simple form, which is derived from the asymptotic analysis of the solution U_m to (1.2). As far as we know, there is less study on the asymptotic of the peak time in a rigorous way in the case of nonzero fluorescence lifetime $\ell > 0$. Then, it is verified numerically that the approximate peak time has an excellent accuracy to the peak time of the solution U_m in (1.2) under the practical range of optical parameters μ_a, D, ℓ, and the depth of target x_{c_3} (see Figure 3.1). Next, we apply the approximate peak time for FDOT. When there is a single point target, we can develop the bisection reconstruction algorithm for the case $\ell > 0$, where the algorithm itself has been already given in [4] for the case $\ell = 0$ and see that the algorithm is less time-consuming, efficient, potentially robust, and accurate. Even the equation (1.6) is written in the case of a single point target, it can be generalized for the case of multiple point targets depending on the parameter $\lambda > 0$ (See (3.8)). Finally, a boundary-scan algorithm is proposed to reconstruct multiple point targets, and it is verified numerically.

The rest of this paper is organized as follows. In Section 2, we introduce the asymptotic behavior of zero fluorescence lifetime solution and obtain the asymptotic behavior of its time integration. In Section 3, we derive the approximate peak time equation and define the approximate peak time. The performance of the approximation is numerically verified. In Section 4, the mathematical properties between the peak time and the location of a target are rigorously studied. Based on this, we propose the bisection reconstruction algorithm and the boundary-scan reconstruction algorithm for the cases of single point and multiple point targets, respectively. In Section 5, several examples are tested to show the efficiency of the proposed reconstruction algorithms. Finally, we conclude in Section 6.

2 Asymptotic behavior of solution

In this section, we consider the asymptotic behavior of the solution U_m to (1.2) for single point and multiple point targets, respectively.

2.1 Single point target

In this subsection, we focus on the single point target case, i.e., $J = 1$ in (1.4). For simplicity, we suppress the superscript (1) of $x_c^{(1)}$ and subscript 1 of c_1 in (1.4). By (1.3), the solution U_m to (1.2) is given as

$$U_m = \mathcal{K} * (\mu f_\ell * u_e) = f_\ell * (\mathcal{K} * [\mu u_e]), \tag{2.1}$$

where $\mathcal{K}$ is the Green function associated with (1.2). Here we denote $u_m := \mathcal{K} * [\mu u_e]$ by the zero lifetime solution, which is independent of fluorescence lifetime $\ell > 0$. For any given $x_d, x_s \in \partial\Omega$, the solution U_m to (2.1) becomes

$$
\begin{aligned}
U_m(x_d, t; x_s) &= \int_0^t \ell^{-1} e^{-\frac{t-s}{\ell}} u_m(x_d, s; x_s) \, \mathrm{d}s \\
&= \ell^{-1} \int_0^t u_m(x_d, s; x_s) \, \mathrm{d}s - \int_0^t \ell^{-2} e^{-\frac{t-s}{\ell}} \left[\int_0^s u_m(x_d, \delta; x_s) \, \mathrm{d}\delta \right] \mathrm{d}s \\
&= \ell^{-1} \int_0^t u_m(x_d, s; x_s) \, \mathrm{d}s - \ell^{-2} \int_0^t \left[\int_0^s u_m(x_d, \delta; x_s) \, \mathrm{d}\delta \right] \mathrm{d}s + O\left(\ell^{-3}\right)
\end{aligned}
\tag{2.2}
$$

4

as $\ell \gg 1$. We define the approximate solution of U_m by

$$
\begin{aligned}
U_m^a(t) &:= \ell^{-1} \int_0^t u_m(s)\,\mathrm{d}s - \ell^{-2} \int_0^t \int_0^s u_m(\delta)\,\mathrm{d}\delta\,\mathrm{d}s \\
&= \ell^{-1} \int_0^t u_m(s)\,\mathrm{d}s - \ell^{-2} \int_0^t (t-s)u_m(s)\,\mathrm{d}s.
\end{aligned}
\tag{2.3}
$$

Now, our aim is to study the asymptotic behaviors of u_m and its time integration. We first give the expression for u_m. The Green function $\mathcal{K}$ is represented by

$$
\mathcal{K}(x, y; t) = \frac{v e^{-v\mu_a t}}{(4\pi v D t)^{\frac{3}{2}}} e^{-\frac{(x_1 - y_1)^2 + (x_2 - y_2)^2}{4vDt}} \mathcal{K}_3(x_3, y_3; t),
\tag{2.4}
$$

where $\mathcal{K}_3$ satisfies the Robin boundary condition, which is

$$
\begin{cases}
\mathcal{K}_3(x_3, y_3; t) = e^{-\frac{(x_3 + y_3)^2}{4vDt}} + e^{-\frac{(x_3 - y_3)^2}{4vDt}} - 2\beta\sqrt{\pi v D t}\, e^{\beta(x_3 + y_3) + \beta^2 v D t}\, \mathrm{erfc}\left(\frac{x_3 + y_3 + 2\beta v D t}{\sqrt{4vDt}}\right), \\
\mathrm{erfc}(\eta) = \frac{2}{\sqrt{\pi}} \int_\eta^\infty e^{-s^2}\,\mathrm{d}s, \quad \eta \in \mathbb{R},
\end{cases}
$$

where x_j denotes j-th component of the three dimensional vector x. For the zero lifetime solution u_m, since the solution of u_e to (1.1) is given as $u_e = D \times \mathcal{K}$, we have the following expression

$$
\begin{aligned}
u_m(x_d, t; x_s) = \frac{c e^{-v\mu_a t}}{16\pi^3 D^2 v} \int_0^t \left((t-s)s\right)^{-\frac{3}{2}} e^{-\frac{|x_d - x_c|^2}{4vD(t-s)}} e^{-\frac{|x_s - x_c|^2}{4vDs}} \\
\times \hat{\mathcal{K}}_3(x_{c_3}; t-s)\hat{\mathcal{K}}_3(x_{c_3}; s)\,\mathrm{d}s,
\end{aligned}
\tag{2.5}
$$

where

$$
\hat{\mathcal{K}}_3(x_{c_3}; t) := 1 - \beta\sqrt{\pi v D t}\, \exp\left(\left(\frac{x_{c_3} + 2\beta v D t}{\sqrt{4vDt}}\right)^2\right) \mathrm{erfc}\left(\frac{x_{c_3} + 2\beta v D t}{\sqrt{4vDt}}\right).
$$

Here $|x|^2 = x_1^2 + x_2^2 + x_3^2$ for $x = (x_1, x_2, x_3) \in \mathbb{R}^3$.

The next lemma describes the asymptotic behavior of u_m for $x_{c_3} \gg 1$ (see [4, Theorem 2.2 and Remark 2.3]).

Lemma 2.1. *Let x_d, $x_s \in \partial\Omega$, and assume that*

$$
\left| |x_d - x_c|^2 - |x_s - x_c|^2 \right| \le Ct \quad \text{for some} \quad C > 0.
\tag{2.6}
$$

Then, u_m satisfies

$$
u_m(t) = u_m^a(t) + O\left(u_m^a(t) x_{c_3}^{-1}\right), \quad x_{c_3} \gg 1,
\tag{2.7}
$$

where

$$
\begin{aligned}
u_m^a(t) :=& \frac{c\exp\left(-\mu_a v t\right)}{8\pi^{\frac{5}{2}} v^{\frac{1}{2}} D^{\frac{3}{2}}} \left(\frac{1}{|x_d - x_c|} + \frac{1}{|x_s - x_c|}\right) t^{-\frac{3}{2}} \\
&\times \exp\left(-\frac{|x_d - x_c|^2 + |x_s - x_c|^2}{2vDt}\right) \left(\frac{x_{c_3}}{x_{c_3} + \beta v D t}\right)^2.
\end{aligned}
\tag{2.8}
$$

In the next lemma, we provide asymptotic behaviors of some integrals, which will be used to derive the asymptotic behavior of $\int_0^t u_m^a(s)\,\mathrm{d}s$ for $\lambda \gg 1$.

Lemma 2.2. *Let $\lambda > 0$. Assume $f_\lambda \in C^1[\delta_1, \infty)$ for some $\delta_1 > 0$, and there exists $C > 0$ such that*

$$|\partial_s f_\lambda(s)| \le C\lambda^{-1}|f_\lambda(s)| \quad \text{for} \quad s \ge \delta_1. \tag{2.9}$$

Then, for any $\delta_2 > \delta_1$,

$$\text{i)} \int_{\delta_1}^{\delta_2} e^{-\lambda\eta} f_\lambda(\eta) \, d\eta = \lambda^{-1} f_\lambda(\delta_1) e^{-\lambda\delta_1} + O\left(\lambda^{-3} f_\lambda(\delta_1) e^{-\lambda\delta_1}\right) \quad \text{as} \quad \lambda \gg 1,$$

$$\text{ii)} \int_{\delta_1}^{\delta_2} e^{-\lambda\eta}(\eta - \delta_1)^{-\frac{1}{2}} f_\lambda(\eta) \, d\eta = \pi^{\frac{1}{2}} \lambda^{-\frac{1}{2}} f_\lambda(\delta_1) e^{-\lambda\delta_1} + O\left(\lambda^{-\frac{5}{2}} f_\lambda(\delta_1) e^{-\lambda\delta_1}\right) \quad \text{as} \quad \lambda \gg 1. \tag{2.10}$$

Proof. By (2.9), we obtain for any $\delta_2 > \delta_1$

$$\int_{\delta_1}^{\delta_2} e^{-\lambda\eta} f_\lambda(\eta) \, d\eta = \lambda^{-1} f_\lambda(\delta_1) e^{-\lambda\delta_1} - \lambda^{-1} e^{-\lambda\delta_2} f_\lambda(\delta_2) + \lambda^{-1} \int_{\delta_1}^{\delta_2} e^{-\lambda\eta} \partial_\eta f_\lambda(\eta) \, d\eta$$

$$= \lambda^{-1} f_\lambda(\delta_1) e^{-\lambda\delta_1} + O\left(\lambda^{-3} f_\lambda(\delta_1) e^{-\lambda\delta_1}\right)$$

as $\lambda \gg 1$, which implies i) in (2.10). On the other hand, we obtain

$$\int_{\delta_1}^{\delta_2} e^{-\lambda\eta}(\eta - \delta_1)^{-\frac{1}{2}} f_\lambda(\eta) \, d\eta = e^{-\lambda\delta_1} \int_0^{\delta_2-\delta_1} e^{-\lambda\eta} \eta^{-\frac{1}{2}} f_\lambda(\eta + \delta_1) \, d\eta$$

$$= e^{-\lambda\delta_1}\left[\int_0^{\delta_2-\delta_1} e^{-\lambda\eta} \eta^{-\frac{1}{2}} f_\lambda(\delta_1) \, d\eta + \int_0^{\delta_2-\delta_1} e^{-\lambda\eta} \eta^{\frac{1}{2}} \partial_\eta f_\lambda(\tilde{\eta}_{\delta_1}) \, d\eta\right] \tag{2.11}$$

$$:= I_1 + I_2$$

for some $\tilde{\eta}_{\delta_1} > \delta_1$. Since

$$I_1 = f_\lambda(\delta_1) e^{-\lambda\delta_1} \int_0^{\delta_2-\delta_1} e^{-\lambda\eta} \eta^{-\frac{1}{2}} \, d\eta = f_\lambda(\delta_1) e^{-\lambda\delta_1}\left[\int_0^\infty - \int_{\delta_2-\delta_1}^\infty\right] e^{-\lambda\eta} \eta^{-\frac{1}{2}} \, d\eta$$

$$= 2\lambda^{-\frac{1}{2}} f_\lambda(\delta_1) e^{-\lambda\delta_1} \int_0^\infty e^{-\eta^2} \, d\eta + O\left(\lambda^{-1} f_\lambda(\delta_1) e^{-\lambda\delta_2}\right) \quad \text{as} \quad \lambda \gg 1,$$

and by (2.9), we obtain

$$|I_2| \le C\lambda^{-1}|f_\lambda(\delta_1)| e^{-\lambda\delta_1} \int_0^{\delta_2-\delta_1} e^{-\lambda\eta} \eta^{\frac{1}{2}} \, d\eta$$

$$= C|f_\lambda(\delta_1)|\lambda^{-1} e^{-\lambda\delta_1}\left[-\lambda^{-1} e^{-\lambda(\delta_2-\delta_1)}(\delta_2 - \delta_1)^{\frac{1}{2}} + \frac{\lambda^{-1}}{2}\int_0^{\delta_2-\delta_1} e^{-\lambda\eta} \eta^{-\frac{1}{2}} \, d\eta\right]$$

$$= O\left(\lambda^{-\frac{5}{2}} f_\lambda(\delta_1) e^{-\lambda\delta_1}\right) \quad \text{as} \quad \lambda \gg 1.$$

This together with (2.11) implies

$$\int_{\delta_1}^{\delta_2} e^{-\lambda\eta}(\eta - \delta_1)^{-\frac{1}{2}} f_\lambda(\eta) \, d\eta = \pi^{\frac{1}{2}} \lambda^{-\frac{1}{2}} f_\lambda(\delta_1) e^{-\lambda\delta_1} + O\left(\lambda^{-\frac{5}{2}} f_\lambda(\delta_1) e^{-\lambda\delta_1}\right)$$

as $\lambda \gg 1$, and the proof of Lemma 2.2 is complete. $\qquad\square$

We are ready to derive the asymptotic behavior of the time integration for u_m^a in (2.8), which is closely related to the behavior of the solution U_m to (1.2). In the next Theorem 2.3, we obtain the asymptotic of

$$\int_0^t u_m^a(s) \, ds = \int_0^t e^{-ks - \frac{\lambda^2}{s}} f(s) \, ds \quad \text{as} \quad \lambda \gg 1,$$

6

where

$$k := \mu_a v, \quad \lambda^2 := \frac{|x_d - x_c|^2 + |x_s - x_c|^2}{2vD},$$

$$f(s) := \frac{c}{8\pi^{\frac{5}{2}} v^{\frac{1}{2}} D^{\frac{3}{2}}} \left(\frac{1}{|x_d - x_c|} + \frac{1}{|x_s - x_c|} \right) s^{-\frac{3}{2}} \left(\frac{x_{c_3}}{x_{c_3} + \beta v D s} \right)^2. \tag{2.12}$$

Theorem 2.3. *Assume $t > \lambda k^{-\frac{1}{2}}$. Then u_m^a of (2.8) satisfies*

$$\int_0^t u_m^a(s) \, \mathrm{d}s = k^{-\frac{3}{4}} (\pi\lambda)^{\frac{1}{2}} u_m^a(\lambda k^{-\frac{1}{2}}) + O\left(\lambda^{-\frac{3}{2}} u_m^a(\lambda k^{-\frac{1}{2}}) \right) \tag{2.13}$$

as $\lambda \gg 1$, where $k > 0$ and λ are as in (2.12).

Proof. Since $t > \lambda k^{-\frac{1}{2}}$, we separate the integral into two parts

$$\int_0^t u_m^a(s) \, \mathrm{d}s = \int_0^t e^{-ks - \frac{\lambda^2}{s}} f(s) \, \mathrm{d}s = \int_0^{\frac{t}{\lambda}} e^{-\lambda \left(k\zeta + \zeta^{-1} \right)} \lambda f(\lambda\zeta) \, \mathrm{d}\zeta$$

$$= \lambda \left[\int_0^{k^{-\frac{1}{2}}} + \int_{k^{-\frac{1}{2}}}^{\frac{t}{\lambda}} \right] e^{-\lambda \left(k\zeta + \zeta^{-1} \right)} f(\lambda\zeta) \, \mathrm{d}\zeta. \tag{2.14}$$

Set a new variable $\eta := k\zeta + \zeta^{-1}$ having

$$\zeta_\pm := \frac{\eta \pm \sqrt{\eta^2 - 4k}}{2k} \quad \text{with} \quad \mathrm{d}\zeta_\pm = \frac{1}{2k} \left[1 \pm \eta(\eta^2 - 4k)^{-\frac{1}{2}} \right] \mathrm{d}\eta.$$

We obtain

$$\int_0^t u_m^a(s) \, \mathrm{d}s = -\lambda \int_{2\sqrt{k}}^\infty e^{-\lambda\eta} f(\lambda\zeta_-) \, \mathrm{d}\zeta_- + \lambda \int_{2\sqrt{k}}^{\eta(\frac{t}{\lambda})} e^{-\lambda\eta} f(\lambda\zeta_+) \, \mathrm{d}\zeta_+$$

$$= -\frac{\lambda}{2k} \int_{2\sqrt{k}}^\infty e^{-\lambda\eta} f(\lambda\zeta_-) \, \mathrm{d}\eta + \frac{\lambda}{2k} \int_{2\sqrt{k}}^\infty e^{-\lambda\eta} f(\lambda\zeta_-) \eta(\eta^2 - 4k)^{-\frac{1}{2}} \, \mathrm{d}\eta \tag{2.15}$$

$$+ \frac{\lambda}{2k} \int_{2\sqrt{k}}^{\eta(\frac{t}{\lambda})} e^{-\lambda\eta} f(\lambda\zeta_+) \, \mathrm{d}\eta + \frac{\lambda}{2k} \int_{2\sqrt{k}}^{\eta(\frac{t}{\lambda})} e^{-\lambda\eta} f(\lambda\zeta_+) \eta(\eta^2 - 4k)^{-\frac{1}{2}} \, \mathrm{d}\eta.$$

We apply Lemma 2.2 with $f_\lambda(s) = f(\lambda s)$ for $s \geq \delta_1 = 2\sqrt{k}$ to obtain

$$\int_0^t u_m^a(s) \, \mathrm{d}s = -\frac{1}{2k} f(\lambda k^{-\frac{1}{2}}) e^{-2\lambda\sqrt{k}} + \frac{\pi^{\frac{1}{2}} \lambda^{\frac{1}{2}}}{2k} f(\lambda k^{-\frac{1}{2}}) 2\sqrt{k} (4\sqrt{k})^{-\frac{1}{2}} e^{-2\lambda\sqrt{k}} + \frac{1}{2k} f(\lambda k^{-\frac{1}{2}}) e^{-2\lambda\sqrt{k}}$$

$$+ \frac{\pi^{\frac{1}{2}} \lambda^{\frac{1}{2}}}{2k} f(\lambda k^{-\frac{1}{2}}) 2\sqrt{k} (4\sqrt{k})^{-\frac{1}{2}} e^{-2\lambda\sqrt{k}} + O\left(\lambda^{-\frac{3}{2}} f(\lambda k^{-\frac{1}{2}}) e^{-2\lambda\sqrt{k}} \right) \tag{2.16}$$

$$= k^{-\frac{3}{4}} (\pi\lambda)^{\frac{1}{2}} f(\lambda k^{-\frac{1}{2}}) e^{-2\lambda\sqrt{k}} + O\left(\lambda^{-\frac{3}{2}} f(\lambda k^{-\frac{1}{2}}) e^{-2\lambda\sqrt{k}} \right)$$

as $\lambda \gg 1$. We remark $\zeta_\pm(2\sqrt{k}) = k^{-\frac{1}{2}}$, and by (2.12), f_λ satisfies the condition (2.9). Since $u_m^a(\lambda k^{-\frac{1}{2}}) = f(\lambda k^{-\frac{1}{2}}) e^{-2\lambda\sqrt{k}}$, we obtain (2.13), and the proof of Theorem 2.3 is complete. □

2.2 Multiple point targets

In this subsection, we turn to consider the asymptotic behavior of U_m defined by (2.1) for the multiple point targets $x_c^{(1)}, x_c^{(2)}, \cdots, x_c^{(J)} \in \Omega$. By using the principle of superposition, the zero lifetime solution, still denoted by u_m, can be defined by

$$u_m(x_d, t; x_s) = \sum_{j=1}^J u_m^{(j)}(x_d, t; x_s), \tag{2.17}$$

7

where x_d, $x_s \in \partial\Omega$, each $u_m^{(j)}$, $j = 1, 2, \cdots, J$, is defined by (2.5) replacing x_c with $x_c^{(j)}$.

The following Corollary gives the asymptotic behaviors of u_m and its time integration.

Corollary 2.4. *Let x_d, $x_s \in \partial\Omega$ and $x_c^{(1)}$, $x_c^{(2)}$, $\cdots$, $x_c^{(J)} \in \Omega$. Assume that there exists some $x_c^{(l)}$, $l = 1, 2, \cdots, J$, such that*

$$|x_d - x_c^{(l)}|^2 + |x_s - x_c^{(l)}|^2 < |x_d - x_c^{(j)}|^2 + |x_s - x_c^{(j)}|^2, \quad 1 \leq j \neq l \leq J, \tag{2.18}$$

and

$$\left| |x_d - x_c^{(l)}|^2 - |x_s - x_c^{(l)}|^2 \right| \leq C^{(l)} t \quad \text{for some} \quad C^{(l)} > 0.$$

Then, we have the asymptotic formula of u_m

$$u_m(t; x_c^{(1)}, x_c^{(2)}, \cdots, x_c^{(J)}) = u_m^{a,(l)}(t)[1 + o(1)] \tag{2.19}$$

as $x_{c3}^{(l)} \gg 1$, where $u_m^{a,(l)}$ can be defined by (2.8) replacing x_c with $x_c^{(l)}$.

Moreover, assuming that $t > \lambda^{(l)} k^{-\frac{1}{2}}$, then

$$\sum_{j=1}^{J} \int_0^t u_m^{a,(j)}(s) \, \mathrm{d}s = k^{-\frac{3}{4}} \left(\pi\lambda^{(l)} \right)^{\frac{1}{2}} u_m^a(\lambda^{(l)} k^{-\frac{1}{2}})[1 + o(1)] \tag{2.20}$$

as $\lambda^{(l)} \gg 1$, where $\lambda^{(l)}$ can be defined by (2.12) replacing x_c with $x_c^{(l)}$.

Proof. As generalizations of Lemma 2.1, for each $x_c^{(j)}$, $j = 1, 2, \cdots, J$ such that $\left| |x_d - x_c^{(j)}|^2 - |x_s - x_c^{(j)}|^2 \right| \leq C^{(j)} t$ for some $C^{(j)} > 0$, then $u_m^{(j)}$ satisfies

$$u_m^{(j)}(t) = u_m^{a,(j)}(t) + O\left(u_m^{a,(j)}(t)(x_{c3}^{(j)})^{-1} \right), \quad x_{c3}^{(j)} \gg 1.$$

It is obvious that the dominant part of each $u_m^{a,(j)}$ is the exponentially small term $\exp\left(-\frac{|x_d - x_c^{(l)}|^2 + |x_s - x_c^{(l)}|^2}{2vDt} \right)$. Under the condition (2.18), we obtain

$$\sum_{j=1}^{J} u_m^{a,(j)}(t) = u_m^{a,(l)}(t)[1 + o(1)],$$

which implies (2.19). Based on this and by the same proof of Theorem 2.3, we obtain (2.20). □

Remark 2.5. *The asymptotic behaviors (2.19) and (2.20) are related to $x_c^{(l)}$ due to (2.18). In other words, we can derive the same asymptotic behaviors of u_m and its time integration for each $x_c^{(l)}$, $l = 1, 2, \cdots, J$, if there always exist x_d, $x_s \in \partial\Omega$ such that (2.18) for each $x_c^{(l)}$, $l = 1, 2, \cdots, J$.*

3   Approximate peak time

In this section, we derive approximate peak time equations and define approximate peak times for the cases of single point and multiple point targets, respectively. The accuracy of the approximate peak times is numerically verified.

By (2.3), we look for an approximate peak time for U_m as t, which satisfies

$$\partial_t U_m^a(t) = \ell^{-1} u_m(t) - \ell^{-2} \int_0^t u_m(s) \, \mathrm{d}s = 0. \tag{3.1}$$

In the following, approximating u_m by (2.7) and (2.19), we consider the cases of single point and multiple point targets, respectively.

3.1 Approximate peak time for single point target

For the single point target, replacing u_m with u_m^a in (3.1) leads to

$$\int_0^t u_m^a(s)\, \mathrm{d}s = \ell u_m^a(t), \tag{3.2}$$

where u_m^a is as in (2.8). By (2.12) and Theorem 2.3, (3.2) becomes

$$\ell e^{-\frac{kt^2+\lambda^2}{t}} f(t) = \ell u_m^a(t) \sim k^{-\frac{3}{4}} (\pi\lambda)^{\frac{1}{2}} f(\lambda k^{-\frac{1}{2}}) e^{-2\lambda\sqrt{k}},$$

and from

$$\left(\frac{x_{c_3} + \beta v D t}{x_{c_3} + \beta v D \lambda k^{-\frac{1}{2}}} \right)^2 \to 1 \quad \text{as} \quad x_{c_3} \gg 1,$$

we can approximate (3.2) by

$$\lambda e^{-\frac{(\sqrt{k}t - \lambda)^2}{t}} = \pi^{\frac{1}{2}} \ell^{-1} t^{\frac{3}{2}}. \tag{3.3}$$

Based on (3.3), we first define the approximate peak time as the root of the approximate peak time equation

$$P(t; \lambda) = 0, \tag{3.4}$$

where $P(t; \lambda)$ is given as

$$P(t;\lambda) := \lambda e^{-\frac{(\sqrt{k}t-\lambda)^2}{t}} - \pi^{\frac{1}{2}}\ell^{-1}t^{\frac{3}{2}}, \; t > \lambda k^{-\frac{1}{2}}. \tag{3.5}$$

Then, we study the unique existence of the approximate peak time and numerically test its applicability to different physical situations.

Theorem 3.1. *Let $x_c \in \Omega$ and $x_d, x_s \in \partial\Omega$, which are assumed to satisfy the constraint (2.6), $x_{c_3} \gg 1$, and $\ell > \pi^{\frac{1}{2}} k^{-\frac{3}{4}} \lambda^{\frac{1}{2}}$. Then, there exists a unique root t_{peak}^a of $P(t)$ such that*

$$P(t) > 0, \; \lambda k^{-\frac{1}{2}} < t < t_{peak}^a \; \text{ and } \; P(t) < 0, \; t > t_{peak}^a.$$

Proof. To show the unique existence of t_{peak}^a, let us first examine the monotonicity of $P(t; \lambda)$ for $t > \lambda k^{-\frac{1}{2}}$. Consider

$$\partial_t P = \lambda e^{-\frac{(\sqrt{k}t-\lambda)^2}{t}} \times \left(-\frac{(kt^2 - \lambda^2)}{t^2} \right) - \frac{3}{2}\pi^{\frac{1}{2}}\ell^{-1}t^{\frac{1}{2}}.$$

Then, we have $\partial_t P < 0$ for $t > \lambda k^{-\frac{1}{2}}$, which means that $P(t; \lambda)$ is a monotonically decreasing function for $t > \lambda k^{-\frac{1}{2}}$. Hence, we only need to show that $P(t; \lambda) > 0$ at $t = \lambda k^{-\frac{1}{2}}$ and $\lim_{t \to \infty} P(t; \lambda) < 0$. The second one is obvious, and the first one follows from

$$P(\lambda k^{-\frac{1}{2}}; \lambda) = \lambda \left(1 - \pi^{\frac{1}{2}}\ell^{-1}k^{-\frac{3}{4}}\lambda^{\frac{1}{2}} \right).$$

The proof of Theorem 3.1 is complete. $\qquad\qquad\qquad\qquad\qquad\qquad\qquad\qquad\qquad\quad\square$

Next, we numerically examine the performance of the approximate peak time for different physical parameters D, μ_a, ℓ, and the depth of the target, x_{c_3}. We evaluate the relative error of the approximate peak time as

$$RelErr_t := \frac{|t_{peak} - t_{peak}^a|}{t_{peak}}, \tag{3.6}$$

where the peak time t_{peak} and the approximate peak time t_{peak}^a are computed from (2.1) and (3.4), respectively. Here, we compute $U_m(x_d, t; x_s)$ using a numerical integration with a time step 0.1 ps, then find the peak time t_{peak} from the discretized time point, which gives the maximum of $U_m(x_d, t; x_s)$. Both t_{peak}, t_{peak}^a

and $RelErr_t$ depend on the physical parameters v, D, μ_a, ℓ, β and the depth x_{c_3}. The parameters D, μ_a, and v depend on the biological tissue types and conditions. Since there is a large variety of the reported values of D and μ_a[2, 25], we choose some representative values for evaluating how the approximation performs under the practical ranges of these parameters. We assume that the refractive index is a fixed value of 1.37 because biological tissues dominantly consist of water, resulting in β only depending on D and the fixed light speed of 0.219 mm/ps. The fluorescence lifetime ℓ depends on the fluorophore molecule and its environment, but the value is usually less than a few nano-seconds for typical organic fluorophore molecules [14]. The target depth x_{c_3} is limited by a detection limit of about 30 mm [24]. If no otherwise specified, we always set $x_{c_3} = 20$ mm and

$$v = 0.219\,\text{mm/ps}, \quad D = 1/3\,\text{mm}, \quad \mu_a = 0.1\,\text{mm}^{-1}, \quad \beta = 0.5493\,\text{mm}^{-1}, \quad \ell = 1000\,\text{ps}, \qquad (3.7)$$

which are typical values in biological tissues. In Figure 3.1, we show the numerical results for fixed S-D pair $\{x_d, x_s\} = \{(14, 10, 0), (6, 10, 0)\}$, the projected location of the target $x_c = (10, 10, x_{c_3})$ and changed x_{c_3}, D, μ_a, ℓ.

Figures 3.1 (a) and (d) indicate that both the peak time and approximate peak time are increasing, while the differences are decreasing with the fluorescence lifetime $\ell > 0$. The decrease of the relative errors of the approximated peak time is consistent with our approximation based on large $\ell \gg 1$ as in (2.2). Figures 3.1 (b) and (e) show that both the peak time, approximate peak time, and the relative errors of the approximate peak time are decreasing with respect to absorption coefficient $\mu_a > 0$. For fixed μ_a, the relative error becomes smaller for smaller D, which is consistent with our approximation based on large $\lambda \gg 1$ as in (2.13). Figure 3.1 (c) shows that both the peak time and approximate peak time are increasing with respect to the depth of point target $x_{c_3} > 0$ because the distance to the target becomes large. Interestingly, the increase is almost linear with the depth, and this observation is consistent with other studies [6, 7]. However, Figure 3.1 (f) indicates no decrease in the relative error in spite of using the approximation given in (2.7). This is the counterpart to our previous result on the approximation peak time for the case of zero fluorescence lifetime $\ell = 0$.
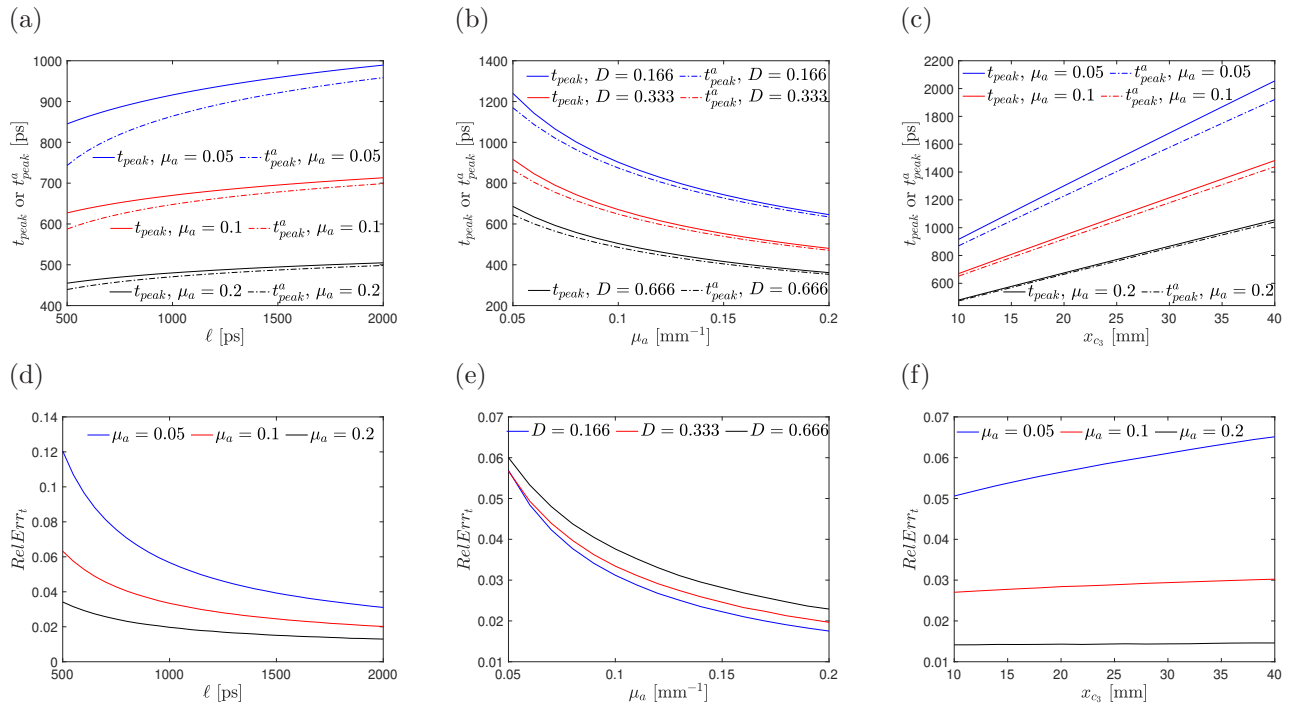

Figure 3.1: Peak time, approximate peak time, and relative error for different physical parameters

3.2 Approximate peak time for multiple point targets

For multiple point targets $x_c^{(j)}$, $j = 1, 2, \cdots, J$, recall Corollary 2.4. Let x_d, $x_s \in \partial\Omega$ satisfying (2.18) for some $x_c^{(l)}$, $l = 1, 2, \cdots, J$. Hence, we can define the approximate peak time $t_{peak}^{a,(l)}$ to $x_c^{(l)}$ as the root of the approximate peak time equation

$$P^{(l)}(t, \lambda^{(l)}) = 0, \tag{3.8}$$

where $P^{(l)}(t, \lambda^{(l)})$ can be defined by (3.5) replacing λ with $\lambda^{(l)} := \left(\frac{|\hat{x}_d - x_c^{(l)}|^2 + |\hat{x}_s - x_c^{(l)}|^2}{2vD} \right)^{\frac{1}{2}}$. From Theorem 3.1, there exists a unique root of $P^{(l)}(t; \lambda^{(l)})$ for $t \in (\lambda^{(l)} k^{-\frac{1}{2}}, \infty)$. As mentioned by Remark 2.5, we can define the unique approximate peak time $t_{peak}^{a,(l)}$ for each $x_c^{(l)}$, $l = 1, 2, \cdots, J$, if x_d, $x_s \in \partial\Omega$ satisfy (2.18).

Next, we numerically verify the accuracy of each approximate peak time $t_{peak}^{a,(l)}$, $l = 1, 2, \cdots, J$, for different S-D pairs. Let us assume there are two point targets, i.e., $J = 2$ in (1.4), with locations $x_c^{(1)} = (5, 10, 20)$, $x_c^{(2)} = (15, 10, 20)$. Setting the physical parameters as (3.7), the peak time t_{peak} and its approximations $t_{peak}^{a,(l)}$, $l = 1, 2$, can be calculated for any S-D pair by using (2.1) and (3.8), respectively. Define a set of S-D pairs as

$$\left\{ \{x_d^{(m,n)}, x_s^{(m,n)}\} := \{(1+m, n, 0), (-1+m, n, 0)\}, \quad m, n = 0, 1, \cdots, 20 \right\}. \tag{3.9}$$

Figure 3.2 (a), (b) and (c) plot the values of the peak time $t_{peak}(x_d^{(m,5)}, x_s^{(m,5)})$ and the approximate peak times $t_{peak}^{a,(1)}(x_d^{(m,5)}, x_s^{(m,5)})$, $t_{peak}^{a,(2)}(x_d^{(m,5)}, x_s^{(m,5)})$ at $m = 0, 1, \cdots, 20$, respectively. We find that $t_{peak}^{a,(1)}$ and $t_{peak}^{a,(2)}$ have symmetric shapes, and give a good approximation to t_{peak} for $m < 10$ and $m > 10$, respectively, since the condition (2.18) is satisfied for $m < 10$ and $m > 10$ to $x_c^{(1)}$ and $x_c^{(2)}$, respectively. In other words, as long as the chosen S-D pair satisfies (2.18) to some $x_c^{(l)}$, $l = 1, 2, \cdots, J$, the defined $t_{peak}^{a,(l)}$ can approximate t_{peak} very well.

Let us define the approximate peak time for these two point targets as follows:

$$t_{peak}^a(x_d^{(m,n)}, x_d^{(m,n)}) := \begin{cases} t_{peak}^{a,(1)}(x_d^{(m,n)}, x_d^{(m,n)}), & m = 0, 1, \cdots, 10, n = 0, 1, \cdots, 20, \\ t_{peak}^{a,(2)}(x_d^{(m,n)}, x_d^{(m,n)}), & m = 11, 12, \cdots, 20, n = 0, 1, \cdots, 20. \end{cases} \tag{3.10}$$

which is plotted for all S-D pairs (3.9) in Figure 3.2 (d). Comparing with t_{peak} shown in Figure 3.2 (e), they have the same shape. The relative error between t_{peak} and t_{peak}^a defined by (3.10) is shown in Figure 3.2 (f), which implies the accuracy of t_{peak}^a defined by (3.10).

4 Reconstruction algorithm

In this section, we study the mathematical properties of the approximate peak time and then numerically verify them. Based on the properties of the peak time, we develop a bisection reconstruction algorithm and a boundary-scan reconstruction algorithm for single point and multiple point targets, respectively, both of which include two stages. In the first stage, we reconstruct the first two coordinates of each target by using the properties of peak time. Then, the third coordinate of each target is reconstructed by solving the approximate peak time equation.

4.1 Properties of peak time related to target location

In this subsection, we rigorously prove some properties of the approximate peak time related to the distance between the target location and the S-D pair, which are also numerically verified to the peak time.

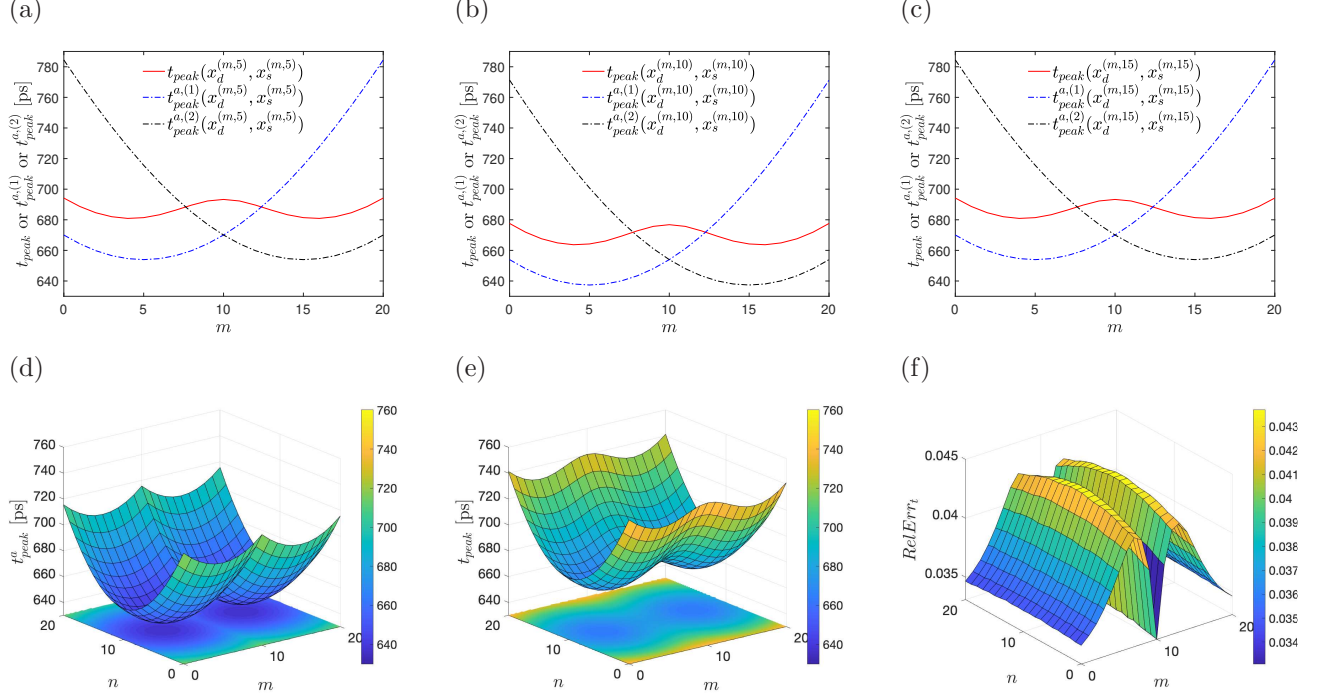We first state the following monotonicity of $P(\lambda; t)$ defined by (3.5) with respect to λ.

Figure 3.2: Peak time, approximate peak time, and relative error for different S-D pairs

Lemma 4.1. *For $t > 0$, $P(\lambda; t)$ is a monotonically increasing function for $\lambda \in (0, tk^{\frac{1}{2}})$.*

Proof. Let us examine the monotonicity of $P(\lambda; t)$ by considering

$$\partial_\lambda P = \left(1 + \frac{2\lambda(\sqrt{k}t - \lambda)}{t}\right) e^{-\frac{(\sqrt{k}t - \lambda)^2}{t}}.$$

Due to the assumption $\lambda < tk^{\frac{1}{2}}$ given in Theorem 2.3, we have $\partial_\lambda P > 0$ for $\lambda \in (0, tk^{\frac{1}{2}})$. □

By showing the properties of t^a_{peak} related to λ, we can obtain the solvability of (x_{c_1}, x_{c_2}) under additional assumptions on S-D pairs as follows.

Theorem 4.2. *For S-D pairs $x_d^{(n)}$, $x_s^{(n)} \in \partial\Omega$, $n = 1, 2$, we have the following equivalence*

$$t^{a,(1)}_{peak} \geq t^{a,(2)}_{peak} \Longleftrightarrow \lambda^{(1)} \geq \lambda^{(2)}, \tag{4.1}$$

where $t^{a,(n)}_{peak} := t^a_{peak}(x_d^{(n)}, x_s^{(n)}; x_c)$ and $\lambda^{(n)} := \lambda(x_d^{(n)}, x_s^{(n)}; x_c)$, $n = 1, 2$. If we assume that S-D pairs satisfy

$$|x_d^{(1)} - x_s^{(1)}| = |x_d^{(2)} - x_s^{(2)}|, \tag{4.2}$$

$t^{a,(2)}_{peak}$ attains its unique minimum when $x_d^{(2)}$ and $x_s^{(2)}$ satisfy

$$x_{c_1} = \frac{x_{d_1}^{(2)} + x_{s_1}^{(2)}}{2}, \quad x_{c_2} = \frac{x_{d_2}^{(2)} + x_{s_2}^{(2)}}{2}. \tag{4.3}$$

where $x_{d_j}^{(2)}$ and $x_{s_j}^{(2)}$, $j = 1, 2$, denote the j-th coordinate of $x_d^{(2)}$ and $x_s^{(2)}$, respectively.

If we further assume that S-D pairs satisfy

$$x_{s_1}^{(1)} - x_{s_1}^{(2)} = x_{d_1}^{(1)} - x_{d_1}^{(2)}, \quad x_{s_2}^{(1)} = x_{s_2}^{(2)}, \quad x_{d_2}^{(1)} = x_{d_2}^{(2)}, \tag{4.4}$$

12

then, $t_{peak}^{a,(1)} = t_{peak}^{a,(2)}$ implies

$$x_{c_1} = \frac{x_{s_1}^{(1)} + x_{d_1}^{(2)}}{2}. \tag{4.5}$$

Similarly, if

$$x_{s_2}^{(1)} - x_{s_2}^{(2)} = x_{d_2}^{(1)} - x_{d_2}^{(2)}, \ \ x_{s_1}^{(1)} = x_{s_1}^{(2)}, \ \ x_{d_1}^{(1)} = x_{d_1}^{(2)}, \tag{4.6}$$

then, $t_{peak}^{a,(1)} = t_{peak}^{a,(2)}$ implies

$$x_{c_2} = \frac{x_{s_2}^{(1)} + x_{d_2}^{(2)}}{2}. \tag{4.7}$$

Proof. By Theorem 3.1 and for $\lambda^{(n)}$, there exists a unique $t_{peak}^{a,(n)}$ satisfying $\lambda^{(n)} < t_{peak}^{a,(n)} k^{\frac{1}{2}}$ such that

$$P(t_{peak}^{a,(n)}; \lambda^{(n)}) = 0, \ \ n = 1, 2. \tag{4.8}$$

We divide the proof of the equivalence (4.1) into two steps. We first prove the equivalence $t_{peak}^{a,(1)} > t_{peak}^{a,(2)} \Leftrightarrow \lambda^{(1)} > \lambda^{(2)}$. Suppose that $t_{peak}^{a,(1)} > t_{peak}^{a,(2)}$. Hence, we have

$$\lambda^{(2)} < t_{peak}^{a,(2)} k^{\frac{1}{2}} < t_{peak}^{a,(1)} k^{\frac{1}{2}}. \tag{4.9}$$

By the proof of Theorem 3.1, we have

$$t_{peak}^{a,(2)} = \overline{t_{peak}^{a,(2)}} = \underline{t_{peak}^{a,(2)}}, \tag{4.10}$$

where

$$\begin{aligned}
\overline{t_{peak}^{a,(2)}} &:= \sup\{t > 0 : P(t'; \lambda^{(2)}) > 0 \ (\lambda^{(2)} k^{-\frac{1}{2}} < t' < t)\}, \\
\underline{t_{peak}^{a,(2)}} &:= \inf\{t > 0 : P(t'; \lambda^{(2)}) < 0 \ (t' > t)\}.
\end{aligned} \tag{4.11}$$

Then, $t_{peak}^{a,(1)} > t_{peak}^{a,(2)}$ implies

$$0 = P(t_{peak}^{a,(2)}; \lambda^{(2)}) > P(t_{peak}^{a,(1)}; \lambda^{(2)}). \tag{4.12}$$

Combining this with $P(t_{peak}^{a,(1)}; \lambda^{(1)}) = 0$, we have

$$P(t_{peak}^{a,(1)}; \lambda^{(1)}) > P(t_{peak}^{a,(1)}; \lambda^{(2)}).$$

By Lemma 4.1 together with (4.9), we obtain $\lambda^{(1)} > \lambda^{(2)}$.

Conversely, we assume that $\lambda^{(1)} > \lambda^{(2)}$, which also gives the condition

$$\lambda^{(2)} < \lambda^{(1)} < t_{peak}^{a,(1)} k^{\frac{1}{2}}.$$

Combining this with Lemma 4.1, we have

$$0 = P(t_{peak}^{a,(1)}, \lambda^{(1)}) > P(t_{peak}^{a,(1)}, \lambda^{(2)}).$$

Since $P(t_{peak}^{a,(2)}, \lambda^{(2)}) = 0$, we arrive at (4.12). Due to

$$\lambda^{(2)} < \lambda^{(1)} < t_{peak}^{a,(1)} k^{\frac{1}{2}} \ \ \text{and} \ \ \lambda^{(2)} < t_{peak}^{a,(2)} k^{\frac{1}{2}},$$

the relation (4.12) implies $t_{peak}^{a,(1)} > t_{peak}^{a,(2)}$ from the proof of Theorem 3.1.

Next, we prove the equivalence $t_{peak}^{a,(1)} = t_{peak}^{a,(2)} \Leftrightarrow \lambda^{(1)} = \lambda^{(2)}$. Assuming that $\lambda^{(1)} = \lambda^{(2)}$, it is obvious that $t_{peak}^{a,(1)} = t_{peak}^{a,(2)}$ by using the uniqueness of the approximate peak time. On the other hand, we assume that $t_{peak}^{a,(1)} = t_{peak}^{a,(2)}$. From (4.8), we have

$$t_{peak}^{a,(1)}(\ln \lambda^{(1)} - \ln \lambda^{(2)}) = (\sqrt{k} t_{peak}^{a,(1)} - \lambda^{(1)})^2 - (\sqrt{k} t_{peak}^{a,(1)} - \lambda^{(2)})^2. \tag{4.13}$$

13

For fixed $\lambda^{(1)}$, the left hand side of (4.13) increases as $\lambda^{(2)} \in (0, t_{peak}^{a,(1)} k^{\frac{1}{2}})$ increases, monotonically. Similarly, the right-hand side of (4.13) decreases monotonically. Hence, there must be $\lambda^{(1)} = \lambda^{(2)}$ in (4.13).

The value $\lambda^{(2)}$ has a unique smallest value whenever $x_d^{(2)}$ and $x_s^{(2)}$ satisfy the condition (4.3). That is, (4.3) gives the condition of taking the minimal approximate peak time. The uniqueness has been proven in Theorem 3.1.

With an additional assumption (4.4), let $L := x_{s_1}^{(1)} - x_{s_1}^{(2)} = x_{d_1}^{(1)} - x_{d_1}^{(2)}$. We have proved the fact that $t_{peak}^{a,(1)} = t_{peak}^{a,(2)}$ implies $\lambda^{(1)} = \lambda^{(2)}$, which gives

$$(x_{d_1}^{(1)} - x_{c_1})^2 + (x_{s_1}^{(1)} - x_{c_1})^2 = (x_{d_1}^{(2)} - x_{c_1})^2 + (x_{s_1}^{(2)} - x_{c_1})^2. \tag{4.14}$$

Substituting $x_{d_1}^{(1)} = L + x_{d_1}^{(2)}$ and $x_{s_1}^{(1)} = L + x_{s_1}^{(2)}$ into above equation, there is a unique solution

$$x_{c_1} = \frac{x_{d_1}^{(2)} + x_{s_1}^{(2)} + L}{2} = \frac{x_{s_1}^{(1)} + x_{d_1}^{(2)}}{2}.$$

Under the assumption (4.6), x_{c_2} can be uniquely determined from (4.14). $\qquad \square$

In the following, we numerically verify that the peak time possesses the same properties given in Theorem 4.2.

Let $x_c = (10, 10, 20)$ and the physical parameters be (3.7). We compute the peak time, the approximate peak time, and the relative error for a set of S-D pairs defined as

$$\left\{ \{x_d^{(m,n)}, x_s^{(m,n)}\} = \{(4+m, n, 0), (-4+m, n, 0)\}, \quad m, n = 0, 1, \cdots, 20 \right\}, \tag{4.15}$$

which are plotted in Figure 4.1. For simplicity, we write

$$t_{peak}^{(m,n)} := t_{peak}(x_d^{(m,n)}, x_s^{(m,n)}; x_c), \quad t_{peak}^{a,(m,n)} := t_{peak}^a(x_d^{(m,n)}, x_s^{(m,n)}; x_c),$$
$$\lambda^{(m,n)} := \lambda(x_d^{(m,n)}, x_s^{(m,n)}; x_c), \quad RelErr_t^{(m,n)} := RelErr_t(x_d^{(m,n)}, x_s^{(m,n)}; x_c).$$

Here, the relative error $RelErr_t^{(m,n)}$ has a similar definition given in (3.6). We mention that each grid point (m, n) in Figure 4.1 (a), (b) and (c) corresponds to $t_{peak}^{(m,n)}$, $t_{peak}^{a,(m,n)}$ and $RelErr_t^{(m,n)}$, respectively.
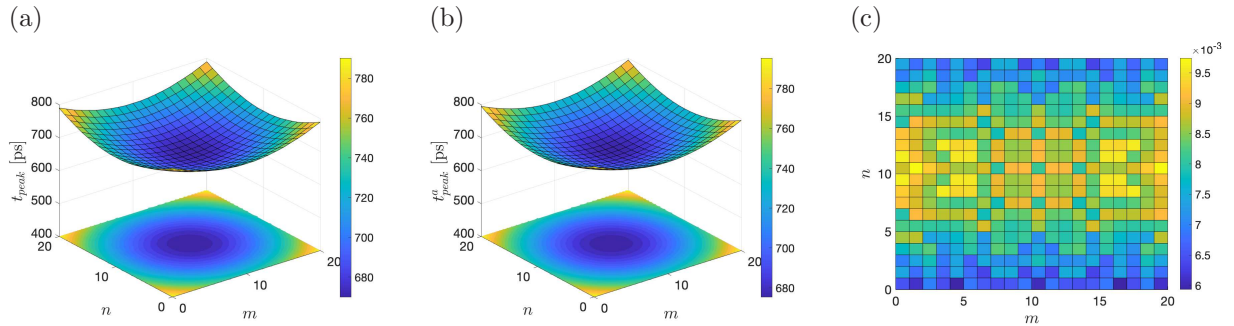

Figure 4.1: (a) peak time, (b) approximate peak time, and (c) relative error for S-D pairs defined by (4.15)

We have the following observations of the peak time from the results shown in Figure 4.1:

(i) Uniqueness: there always exists only one peak time for each S-D pair defined by (4.15).

(ii) Order relation: $t_{peak}^{(m,n)}$ decreases as $(m, n) \to (10, 10)$, since $\lambda^{(m,n)}$ decreases as $(m, n) \to (10, 10)$. We obtain the smallest peak time at $\{x_d^{(10,10)}, x_s^{(10,10)}\}$, which satisfies $x_{d_1}^{(10,10)} + x_{s_1}^{(10,10)} = 2x_{c_1}$, $x_{d_2}^{(10,10)} + x_{s_2}^{(10,10)} = 2x_{c_2}$, i.e., (4.3).

14

(iii) Symmetry: for any (m_1, n_1) and (m_2, n_2) satisfying $\lambda^{(m_1, n_1)} = \lambda^{(m_2, n_2)}$, we observe $t_{peak}^{(m_1, n_1)} = t_{peak}^{(m_2, n_2)}$ from the circular contour shape of the peak times as shown in the bottom plot of Figure 4.1 (a). It is easy to verify the solvability of (x_{c_1}, x_{c_2}) given in (4.5) and (4.7), since the center of the circular contour shape is (x_{c_1}, x_{c_2}).

(iv) Accuracy: the relative error shown in Figure 4.1 (c) indicates a good approximation of the approximate peak time.

Despite the limited numerical results, it is reasonable to use the approximate peak time equation and the properties of the approximate peak time to formulate a scheme reconstructing the location of the unknown point target. Hence, unless specified, we do not distinguish the peak time and the approximate peak time in the following parts. Here, we remark that we will set S-D pairs satisfying the assumption (4.4) or (4.6) in the scheme since (4.4) and (4.6) directly imply (4.2).

4.2 Bisection reconstruction algorithm for reconstructing single point target

For the single point target x_c, the properties of the peak time in Theorem 4.2 only depend on (x_{c_1}, x_{c_2}). Hence, we divide the reconstruction scheme into the following two stages:

Stage 1: Let (x_{c_1}, x_{c_2}) be inside of a rectangular region of interest (ROI). By using the peak time as an index, we use the bisection method to gradually shrink ROI and stop by some criterion. We let the center of the updated ROI be the reconstruction $(x_{c_1}^{inv}, x_{c_2}^{inv})$.

Stage 2: Substituting a set of parameters $x_d, x_s \in \partial\Omega$, $t = t_{peak}(x_d, x_s; x_c)$ and $(x_{c_1}, x_{c_2}) = (x_{c_1}^{inv}, x_{c_2}^{inv})$ into (3.5), the depth x_{c_3} can be reconstructed by finding the positive root of (3.4).

Now, we give a detailed explanation of **Stage 1**. Let ROI $:= (x_l, x_r) \times (x_b, x_t) \subset \partial\Omega$. We define four S-D pairs with $L > 0$ as

$$\begin{aligned} \{x_d^{(1)}, x_s^{(1)}\} &:= \left\{(x_l + \tfrac{L}{2}, x_b, 0), (x_l - \tfrac{L}{2}, x_b, 0)\right\}, \{x_d^{(2)}, x_s^{(2)}\} := \left\{(x_l + \tfrac{L}{2}, x_b, 0), (x_r - \tfrac{L}{2}, x_b, 0)\right\}, \\ \{x_d^{(3)}, x_s^{(3)}\} &:= \left\{(x_r + \tfrac{L}{2}, x_t, 0), (x_r - \tfrac{L}{2}, x_t, 0)\right\}, \{x_d^{(4)}, x_s^{(4)}\} := \left\{(x_l + \tfrac{L}{2}, x_t, 0), (x_l - \tfrac{L}{2}, x_t, 0)\right\}. \end{aligned} \quad (4.16)$$

By comparing the order relation of four corresponding peak times $t_{peak}^{(n)} := t_{peak}(x_d^{(n)}, x_d^{(n)}; x_c)$, $n = 1, 2, 3, 4$, we halve the current ROI and obtain an updated ROI, still denoted by ROI $= (x_l, x_r) \times (x_b, x_t)$. Then, we repeat to set four S-D pairs as (4.16) and compare the order relation of the peak times. The algorithm breaks out if a criterion is satisfied. We refer to this scheme as Algorithm 1. Here, we will use the symbol "$\leftarrow$" to represent the update.

It is obvious that there exists a unique reconstruction $(x_{c_1}^{inv}, x_{c_2}^{inv})$ in **Stage 1**. We state the following unique existence of reconstruction $x_{c_3}^{inv}$ from given t_{peak}.

Theorem 4.3. *Let x_c^* be the true location. Assume that $\ell > \pi^{\frac{1}{2}} k^{-\frac{3}{4}} (\lambda^*)^{\frac{1}{2}}$ with $\lambda^* := \lambda(x_d, x_s, x_c^*)$. For given peak time t_{peak}, there exists a unique positive reconstruction $x_{c_3}^{inv}$ such that $\lambda^{inv} < t_{peak} k^{\frac{1}{2}}$ and $P(\lambda^{inv}; t_{peak}) = 0$, where $\lambda^{inv} := \lambda(x_d, x_s, x_c^{inv})$ and $P(\lambda; t)$ are defined by (2.12) and (3.5), respectively.*

Proof. Due to $x_{c_3} > 0$, proving the uniqueness of $x_{c_3}^{inv}$ is equivalent to proving the uniqueness of λ^{inv}. From Lemma 4.1, we obtain that $P(\lambda; t_{peak})$ is monotonically increasing for $\lambda \in (0, t_{peak} k^{\frac{1}{2}})$. Due to $P(0; t_{peak}) < 0$, we only need to compute the value $P(\lambda; t_{peak})$ at $\lambda = t_{peak} k^{\frac{1}{2}}$,

$$P(t_{peak} k^{\frac{1}{2}}; t_{peak}) = t_{peak} k^{\frac{1}{2}} - \pi^{\frac{1}{2}} \ell^{-1} t_{peak}^{\frac{3}{2}} > t_{peak} k^{\frac{1}{2}} + k^{\frac{3}{4}} (\lambda^*)^{-\frac{1}{2}} t_{peak}^{\frac{3}{2}} > 0,$$

which implies the unique existence of λ^{inv}. From (2.12), we obtain that there exists a unique $x_{c_3}^{inv}$. $\qquad\square$

Algorithm 1 Reconstruct (x_{c_1}, x_{c_2}) by using the bisection method

---

Input: ROI $= (x_l, x_r) \times (x_b, x_t)$, tolerances $\epsilon_1, \epsilon_2 > 0$ and distance L.

Step 1 Define four S-D pairs by (4.16).

Step 2 Compute $t_{peak}^{(n)}$, $n = 1, 2, 3, 4$, and update ROI.

1a) If $t_{peak}^{(1)} = t_{peak}^{(2)} = t_{peak}^{(3)} = t_{peak}^{(4)}$, break the loop and output $x_{c_1}^{inv} = \frac{x_l+x_r}{2}$, $x_{c_2}^{inv} = \frac{x_b+x_t}{2}$.

2a) If $t_{peak}^{(1)} = t_{peak}^{(2)} < t_{peak}^{(3)} = t_{peak}^{(4)}$, output $x_{c_1}^{inv} = \frac{x_l+x_r}{2}$, update $x_t \leftarrow \frac{x_b+x_t}{2}$, ROI $\leftarrow (x_b, x_t)$, break the loop and go to Algorithm 2.

2b) If $t_{peak}^{(1)} = t_{peak}^{(2)} > t_{peak}^{(3)} = t_{peak}^{(4)}$, output $x_{c_1}^{inv} = \frac{x_l+x_r}{2}$, update $x_b \leftarrow \frac{x_b+x_t}{2}$, ROI $\leftarrow (x_b, x_t)$, break the loop and go to Algorithm 2.

2c) If $t_{peak}^{(1)} = t_{peak}^{(4)} < t_{peak}^{(2)} = t_{peak}^{(3)}$, output $x_{c_2}^{inv} = \frac{x_b+x_t}{2}$, update $x_r \leftarrow \frac{x_l+x_r}{2}$, ROI $\leftarrow (x_l, x_r)$, break the loop and go to Algorithm 2.

2d) If $t_{peak}^{(1)} = t_{peak}^{(4)} > t_{peak}^{(2)} = t_{peak}^{(3)}$, output $x_{c_2}^{inv} = \frac{x_b+x_t}{2}$, update $x_l \leftarrow \frac{x_l+x_r}{2}$, ROI $\leftarrow (x_l, x_r)$, break the loop and go to Algorithm 2.

3a) If $t_{peak}^{(1)} < \{t_{peak}^{(2)}, t_{peak}^{(3)}, t_{peak}^{(4)}\}$, update $x_r \leftarrow \frac{x_l+x_r}{2}$, $x_t \leftarrow \frac{x_b+x_t}{2}$, ROI $\leftarrow (x_l, x_r) \times (x_b, x_t)$.

3b) If $t_{peak}^{(2)} < \{t_{peak}^{(1)}, t_{peak}^{(2)}, t_{peak}^{(4)}\}$, update $x_l \leftarrow \frac{x_l+x_r}{2}$, $x_t \leftarrow \frac{x_b+x_t}{2}$, ROI $\leftarrow (x_l, x_r) \times (x_b, x_t)$.

3c) If $t_{peak}^{(3)} < \{t_{peak}^{(1)}, t_{peak}^{(2)}, t_{peak}^{(4)}\}$, update $x_l \leftarrow \frac{x_l+x_r}{2}$, $x_b \leftarrow \frac{x_b+x_t}{2}$, ROI $\leftarrow (x_l, x_r) \times (x_b, x_t)$.

3d) If $t_{peak}^{(4)} < \{t_{peak}^{(1)}, t_{peak}^{(2)}, t_{peak}^{(3)}\}$, update $x_r \leftarrow \frac{x_l+x_r}{2}$, $x_b \leftarrow \frac{x_b+x_t}{2}$, ROI $\leftarrow (x_l, x_r) \times (x_b, x_t)$.

Step 3 Compute $Err_1 := x_r - x_l$, $Err_2 := x_t - x_b$ and check stop criterion.

If $Err_1 \leq \epsilon_1$, $Err_2 \leq \epsilon_2$, stop and output $x_{c_1}^{inv} = \frac{x_l+x_r}{2}$, $x_{c_2}^{inv} = \frac{x_b+x_t}{2}$.

If $Err_1 > \epsilon_1$, $Err_2 \leq \epsilon_2$, output $x_{c_2}^{inv} = \frac{x_b+x_t}{2}$, go to Algorithm 2 with ROI $:= (x_l, x_r)$.

If $Err_1 \leq \epsilon_1$, $Err_2 > \epsilon_2$, output $x_{c_1}^{inv} = \frac{x_l+x_r}{2}$, go to Algorithm 2 with ROI $:= (x_b, x_t)$.

If $Err_1 > \epsilon_1$, $Err_2 > \epsilon_2$, go to **Step 1.**

Algorithm 2 Reconstruct x_{c_1} or x_{c_2} after the dimensionality reduction

---

Input: Reconstruction $x_{c_2}^{inv}$, ROI$=(x_l, x_r)$, tolerance ϵ_1 and distance L.

Step 1 Define S-D pairs $\{x_d^{(n)}, x_s^{(n)}\}$, $n = 1, 2$, by (4.16).

Step 2 Compare $t_{peak}^{(1)}$ and $t_{peak}^{(2)}$ and update ROI.

If $t_{peak}^{(1)} = t_{peak}^{(2)}$, break the loop and output $x_{c_1}^{inv} = \frac{x_l+x_r}{2}$.

If $t_{peak}^{(1)} < t_{peak}^{(2)}$, update $x_r \leftarrow \frac{x_l+x_r}{2}$, ROI $\leftarrow (x_l, x_r)$.

If $t_{peak}^{(1)} > t_{peak}^{(2)}$, update $x_l \leftarrow \frac{x_l+x_r}{2}$, ROI $\leftarrow (x_l, x_r)$.

Step 3 Compute $Err_1 = x_r - x_l$ and check stop criterion.

If $Err_1 \leq \epsilon_1$, break the loop and output $x_{c_1}^{inv} = \frac{x_l+x_r}{2}$. Otherwise, go to **Step 1**.

(Note: The case of inputting $x_{c_1}^{inv}$, ROI $= (x_b, x_t)$, ϵ_2 and L can be done in the same way.)

4.3 Boundary-scan algorithm for reconstructing multiple point targets

In this subsection, we propose a boundary-scan method for reconstructing the locations of the multiple point targets $x_c^{(1)}$, $x_c^{(2)}$, $\cdots$, $x_c^{(J)}$, which are assumed to be well-separated.

For each $x_c^{(l)}$, $l = 1, 2, \cdots, J$, the relation between $x_c^{(l)}$ and the approximate peak time $t_{peak}^{a,(l)}$ defined by (3.8) must be the same as described in Theorem 4.2, if we further assume that the S-D pair $\{x_d, x_s\}$ also satisfies (2.18). In this case, $t_{peak}^{a,(l)}$ becomes smaller and smaller as $\{x_d, x_s\}$ gets closer and closer to $x_c^{(l)}$, where the distance between x_d and x_s is fixed. Furthermore, it reaches its minimum when

$$x_{c_1}^{(l)} = \frac{x_{d_1} + x_{s_1}}{2}, \quad x_{c_2}^{(l)} = \frac{x_{d_2} + x_{s_2}}{2}. \tag{4.17}$$

As S-D pair $\{x_d, x_s\}$ moves, if there is another target $x_c^{(k)}$, $1 \le k \ne l \le J$, such that

$$|x_d - x_c^{(k)}|^2 + |x_s - x_c^{(k)}|^2 < |x_d - x_c^{(j)}|^2 + |x_s - x_c^{(j)}|^2, \quad 1 \le j \ne k \le J,$$

we can define its approximate peak time $t_{peak}^{a,(k)}$ by (3.8), which will have the same properties of $t_{peak}^{a,(l)}$ as described above when we move $\{x_d, x_s\}$.

For the peak time t_{peak}, recall the numerical verification given in Subsection 3.2. From Figure 3.2 (d) and (e), we can observe that both t_{peak}^a and t_{peak} become smaller and smaller as (m, n) approaches $(5, 10)$ or $(15, 10)$. They reach local minima at $(m, n) = (5, 10)$ and $(m, n) = (15, 10)$, because the S-D pairs $\{x_d^{(5,10)}, x_s^{(5,10)}\}$ and $\{x_d^{(15,10)}, x_s^{(15,10)}\}$ are the nearest S-D pairs of (3.9) to targets $x_c^{(1)}$ and $x_c^{(2)}$, respectively. Furthermore, $\{x_d^{(5,10)}, x_s^{(5,10)}\}$ and $\{x_d^{(15,10)}, x_s^{(15,10)}\}$ satisfy (4.17) for $x_c^{(1)}$ and $x_c^{(2)}$, respectively. From the relative error between t_{peak}^a and t_{peak} shown in Figure 3.2 (f), we reasonably speculate that t_{peak} approximately satisfies the approximate peak time equation (3.8) to any $x_c^{(j)}$, $j = 1, 2$, where the chosen S-D pair satisfies (2.18).

From the above discussion, the key point of reconstructing the first two coordinates of the targets is to search for the locally minimal peak time. Before proposing the reconstruction algorithm, we define the well-separated multiple point targets as follows.

Definition 4.4. *Let $x_c^{(j)} \in \Omega$, $j = 1, 2, \cdots, J$, be the locations of unknown point targets, where $(x_{c_1}^{(j)}, x_{c_2}^{(j)}) \in$ ROI $:= (x_l, x_r) \times (x_b, x_t)$. We define a set Ξ of S-D pairs as*

$$\Xi := \Big\{ \{x_d^{(m,n)}, x_s^{(m,n)}\} : \{(x_l + \frac{L}{2} + m\frac{x_r - x_l}{M}, x_b + n\frac{x_t - x_b}{N}, 0), (x_l - \frac{L}{2} + m\frac{x_r - x_l}{M}, x_b + n\frac{x_t - x_b}{N}, 0)\}$$

$$m = 0, 1, \cdots, M, n = 0, 1, \cdots, N, L > 0 \Big\}. \tag{4.18}$$

Let us further assume that there is a unique peak time for each $\{x_d^{(m,n)}, x_s^{(m,n)}\} \in \Xi$. Then, there exists a set $\mathcal{P}$ of the peak times corresponding to Ξ. We say that these J unknown point targets are well-separated if there are J local minimums in $\mathcal{P}$ for J multiple point targets

$$t_{peak}^{min,(j)} := t_{peak}^{min}(x_d^{min,(j)}, x_s^{min,(j)}; x_c^{(1)}, \cdots, x_c^{(J)}), \quad j = 1, 2, \cdots, J, \tag{4.19}$$

where the S-D pair $\{x_d^{min,(j)}, x_s^{min,(j)}\} \in \Xi$ is the S-D pair of the smallest distance from the j-th target in Ξ.

We propose a boundary-scan reconstruction algorithm to reconstruct well-separated multiple point targets $x_c^{(j)}$, $1 \le j \le J$, as in Algorithm 3.

Algorithm 3 Boundary-scan reconstruction algorithm for reconstructing multiple point targets

Input: ROI=$(x_l, x_r) \times (x_b, x_t)$, distance L of S-D pair.

Step 1 Scan ROI by using S-D pairs (4.18) and record the peak times $t_{peak}(x_d^{(m,n)}, x_s^{(m,n)})$, $m = 0, 1, \cdots, M$, $n = 0, 1, \cdots, N$.

Step 2 Reconstruct $(x_{c_1}^{(j)}, x_{c_2}^{(j)})$, $j = 1, 2, \cdots, J$, by

$$x_{c_1}^{(j),inv} := \frac{x_{s_1}^{min,(j)} + x_{d_1}^{min,(j)}}{2}, \qquad x_{c_2}^{(j),inv} := \frac{x_{s_2}^{min,(j)} + x_{d_2}^{min,(j)}}{2}, \tag{4.20}$$

where $\{x_d^{min,(j)}, x_s^{min,(j)}\}$ is a S-D pair of Ξ at which peak time takes the local minimum $t_{peak}^{min,(j)}$.

Step 3 Reconstruct $x_{c_3}^{(j)}$, $j = 1, 2, \cdots, J$, by solving (3.8) for given $\{x_d, x_s\} = \{x_d^{min,(j)}, x_s^{min,(j)}\}$, $t = t_{peak}^{min,(j)}$ and $(x_{c_1}^{(j)}, x_{c_2}^{(j)}) = (x_{c_1}^{(j),inv}, x_{c_2}^{(j),inv})$.

5 Numerical experiments

In this section, we apply the proposed bisection reconstruction algorithm and boundary-scan reconstruction algorithm to the numerical experiments of single point and multiple point targets, respectively. In all experiments, we set the physical parameters as (3.7).

Usually, noise, specifically time jitters, is unavoidable in the measurements. We perturb t_{peak} by

$$t_{peak}^{\delta} := \left(1 + \hat{\delta} \times (2 \times \text{rand}(1) - 1)\right) \times t_{peak}, \tag{5.1}$$

where $\hat{\delta}$ is the relative noise level, and rand(1) generates a uniformly distributed random number on the interval $(0, 1)$. We compute the relative error of the reconstruction by the following formula:

$$RelErr = \sum_{j=1}^{J} \frac{|x_c^{(j)} - x_c^{(j),inv}|}{|x_c^{(j)}|}, \tag{5.2}$$

where $x_c^{(j)}$ and $x_c^{(j),inv}$ are the actual and reconstructed location of the j-th target, respectively.

Let us first consider the single point target case and suppress the superscript (j) of $x_c^{(j)}$. We denote by ROI^{inv} the final ROI when the stop criteria of Algorithm 1 and Algorithm 2 are satisfied.

Example 5.1. *Let $x_c = (7, 17, 20)$. By setting* ROI=$(0, 20) \times (0, 20)$, $L = 8$ *and $\epsilon_1 = \epsilon_2 = 0.1$ in Algorithm 1, we show the results of numerical reconstructions for different noise levels in Table 1.*

Table 1: Reconstructions for different noise levels and fixed tolerances $\epsilon_1 = \epsilon_2 = 0.1$

x_c	$\hat{\delta}$	x_c^{inv}	$RelErr$	ROI^{inv}
	0	$(7.03, 17.03, 19.83)$	6.46e-03	$(6.88, 7.19) \times (16.88, 17.19)$
$(7, 17, 20)$	0.1%	$(6.76, 17.30, 19.79)$	1.62e-02	$(6.72, 6.80) \times (17.27, 17.34)$
	1%	$(7.54, 16.99, 19.68)$	2.31e-02	$(7.50, 7.58) \times (16.95, 17.03)$
	5%	$(7.85, 17.30, 19.08)$	4.74e-02	$(7.81, 7.89) \times (17.27, 17.34)$

For noise-free peak time ($\hat{\delta} = 0$), the reconstruction is very close to the actual location, and its first two coordinates are also included in ROI^{inv}, which shows that the proposed algorithm is accurate. Considering

the case of $\hat{\delta} > 0$, although the first two coordinates of the reconstructions are not included in ROI^{inv}, they are still close to the true coordinates. The relative errors of these reconstructions from the noisy peak time are still marginal, less than a few percent.

We mention that the maximum number of shrinks is 8 times for $\epsilon_1 = \epsilon_2 = 0.1$ in **Stage** 1. Next, we reduce the number of shrinks by setting larger tolerances $\epsilon_1 = \epsilon_2 = 1.25$ in Example 5.1. We can still have reasonable numerical results, which are shown in Table 2.

Table 2: Reconstructions for different noise levels and fixed tolerances $\epsilon_1 = \epsilon_2 = 1.25$

x_c	$\hat{\delta}$	x_c^{inv}	$RelErr$	ROI^{inv}
	0	$(6.88, 16.88, 19.81)$	9.51e-03	$(6.25, 7.50) \times (16.25, 17.50)$
$(7, 17, 20)$	0.1%	$(6.88, 16.88, 19.85)$	8.06e-03	$(6.25, 7.50) \times (16.25, 17.50)$
	1%	$(8.13, 16.88, 20.07)$	4.38e-02	$(7.50, 8.75) \times (16.25, 17.50)$
	5%	$(8.13, 16.88, 20.56)$	4.65e-02	$(7.50, 8.75) \times (16.25, 17.50)$

For $\epsilon_1 = \epsilon_2 = 1.25$, the number of shrinks reduces to 4 times in **Stage** 1. Compared with the results shown in Table 1, we obtain that a finite number of shrinks can also give a good result. Now, ROI^{inv} contains the true location of target for $\hat{\delta} = 0.1\%$. In this case, the relative error is smaller than the one shown in Table 1. However, the true location of the target is not included in ROI^{inv} for $\hat{\delta} = 1\%$ and $\hat{\delta} = 5\%$. It is easy to reason that there is a false shrink occurred at the third shrink. Even in this case, we can get the reconstructions similar to Table 1. In short, larger tolerances for larger noise levels may result in a much better reconstruction of the first two coordinates $(x_{c_1}^{inv}, x_{c_2}^{inv})$. Moreover, the reconstruction of the depth $x_{c_3}^{inv}$ is less affected by the reconstruction $(x_{c_1}^{inv}, x_{c_2}^{inv})$.

The next experiment is to verify the proposed algorithm for a deeply embedded target.

Example 5.2. *Let* $x_c = (6, 11, 30)$*. We show the results of numerical reconstructions for different noise levels in Table 3 with the same inputs as Example 5.1.*

Table 3: Reconstructions for different noise levels and fixed tolerances $\epsilon_1 = \epsilon_2 = 0.1$

x_c	$\hat{\delta}$	x_c^{inv}	$RelErr$	ROI^{inv}
	0	$(6.09, 10.78, 30.17)$	9.06e-03	$(5.94, 6.25) \times (10.63, 10.94)$
$(6, 11, 30)$	0.1%	$(5.66, 11.37, 30.17)$	1.62e-02	$(5.63, 5.70) \times (11.33, 11.41)$
	1%	$(7.54, 11.99, 30.02)$	5.63e-02	$(7.50, 7.58) \times (11.95, 12.03)$
	5%	$(7.85, 17.30, 29.79)$	2.02e-01	$(7.81, 7.89) \times (17.27, 17.34)$

For $\hat{\delta} = 0$, we obtain a similar result as Example 5.1, that the reconstruction is very close to the true location. For $\hat{\delta} = 0.1\%$ and $\hat{\delta} = 1\%$, the reconstructions approximate the actual location within small relative errors. The reconstruction becomes worse for $\hat{\delta} = 5\%$, since the peak time is more delayed as the target depth increases, causing an increase in the order of noise. Comparing the results shown in Example 5.1, even for a deeper unknown target, the reconstruction $x_{c_3}^{inv}$ is less affected by the noise.

Next, we use the following numerical example to verify the performance of Algorithm 3 for reconstructing the locations of two unknown point targets.

Example 5.3. *Let* $x_c^{(1)} = (3.3, 5.2, 16)$, $x_c^{(2)} = (17.4, 16.7, 18)$ *and* $\text{ROI} := (0, 20) \times (0, 20)$*. We choose the S-D pairs as (4.18) for* $M = N = 20$, $L = 2$*. The numerical results are shown in Table 4 for different noise levels.*

From Figure 5.1, there exist two local minima $t_{peak}^{min,(1)} = 546.1$ and $t_{peak}^{min,(2)} = 603.5$ measured by S-D pairs $\{x_d^{(3,5)}, x_s^{(3,5)}\}$ and $\{x_d^{(17,17)}, x_s^{(17,17)}\}$, respectively, where the scanning S-D pairs are defined by (4.18).

Table 4: Reconstructions for different noise levels in Example 5.3

$x_c^{(1)}, x_c^{(2)}$	$\hat{\delta}$	$x_c^{(1),inv}$	$x_c^{(2),inv}$	$RelErr$
	0	$(3.00, 5.00, 15.67)$	$(17.00, 17.00, 17.72)$	4.75e-02
$(3.3, 5.2, 16), (17.4, 16.7, 18)$	0.1%	$(3.00, 5.00, 15.71)$	$(17.00, 17.00, 17.79)$	4.51e-02
	1%	$(3.00, 6.00, 15.70)$	$(18.00, 17.00, 17.84)$	7.58e-02

Hence, we can reconstruct these two point targets by using Algorithm 3. For the measured peak times containing noise, we first apply the moving average method with a 3×3 grid to smooth the noisy peak times since the algorithm will fail due to the presence of several local minimal peak times. For instance, looking at the cross-section of the peak time, the noisy peak time, and the smoothed noisy peak time shown in Figure 5.2, several local minimal peak times in $t_{peak}^{\delta}(x_d^{(m,5)}, x_s^{(m,5)})$ and $t_{peak}^{\delta}(x_d^{(m,17)}, x_s^{(m,17)})$ for $m = 0, 1, \cdots, 20$ are clearly visible. After smoothing the noisy peak times, we can distinguish two local minima in the noisy peak times $t_{peak}^{\delta}(x_d, x_s)$, $\{x_d, x_s\} \in \Xi$. Then, we can reconstruct the locations of targets with a similar discussion for the noise-free peak times. The numerical results verify that the proposed algorithm is feasible to reconstruct the locations of multiple point targets.
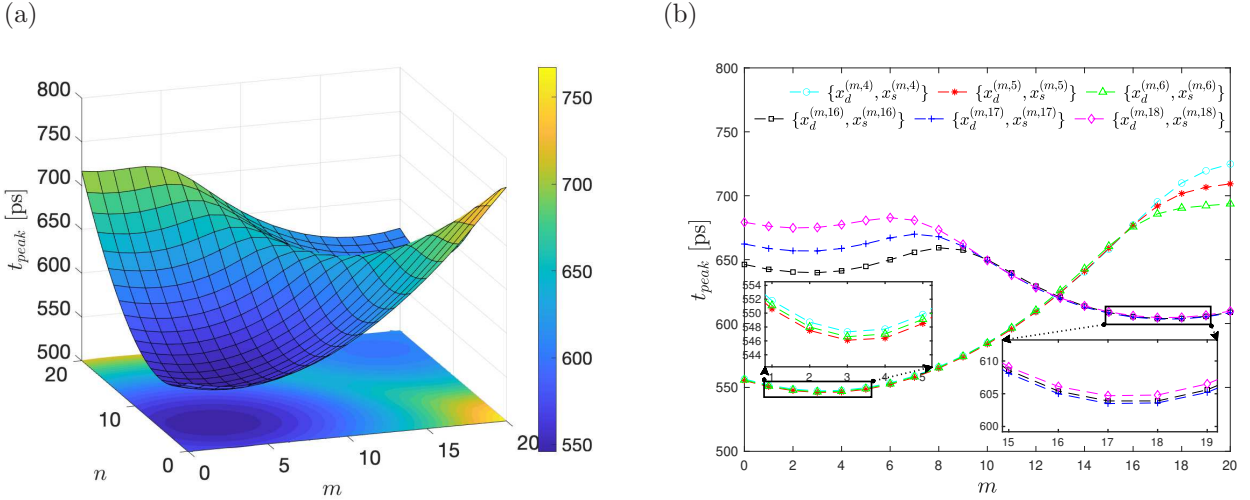
(a)

(b)

Figure 5.1: Noise-free peak times measured by different S-D pairs (4.18) in Example 5.3: (a) 3D contour plot of peak times for $m, n = 0, 1, \cdots, 20$, (b) peak times for $m = 0, 1, \cdots, 20$, $n = 4, 5, 6, 16, 17, 18$

6 Conclusions and future work

In this paper, we studied the reconstruction of the locations of unknown point targets from peak times, which is the time when the temporal response function $U_m(x_d, t; x_s)$ reaches its maximum for a given S-D pair $\{x_d, x_s\}$ on the measurement surface. Further, we considered the peak time for the nonzero lifetime $\ell > 0$ as an extension of our previous paper [4]. Analyzing the asymptotic behavior of U_m, we derived the approximate peak time equation as a nonlinear equation and could define the approximate peak time by its positive root. We proved the properties of approximate peak time (uniqueness, order relation, symmetry, and accuracy) and provided numerical verification of them. Based on these analyses, we proposed bisection reconstruction and boundary-scan algorithms to reconstruct the location of the point targets. We remark on the advantage of considering the peak time. The peak time is uniquely and visibly identified. It is the least noisy data point in $U_m(x_d, t; x_s)$, making it potentially robust for reconstruction.
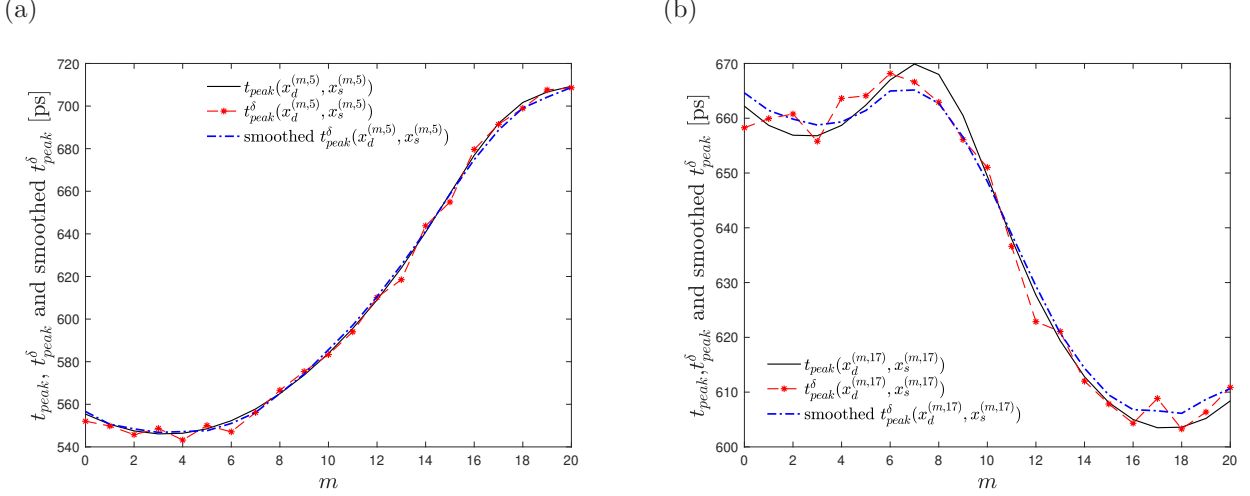
(a)   (b)

Figure 5.2: Peak times, noisy peak times ($\hat\delta = 0.1\%$) and smoothed noisy peak times for $m = 0, 1, 2, \cdots, 20$ and $n = 5, 17$

The novelties of this paper can be summarized as follows

- The case of $\ell > 0$ makes the mathematical model (1.1)–(1.2) better fit the physical processes of FDOT.

- We found no other theoretical study considering the effect of ℓ on the peak time and defining the approximate peak time. The obtained analytical result is reliable and convenient to be applied to our inverse problem.

- The proposed bisection reconstruction and boundary-scan algorithms are less time-consuming, efficient, robust, and accurate for identifying the locations of the point targets without any regularization.

We can further say that based on our asymptotic analysis, we have established reconstructing the locations of multiple points targets using the relation between the peak time and the S-D pairs. In the analysis, the distance function $d(x_c, t) := (|x_d - x_c|^2 + |x_s - x_c|^2)/t$ plays the most important role, where $\{x_d, x_s\}$ is the S-D pair. Actually, the nearest point target x_c to $\{x_d, x_s\}$ is on the sphere centered at $(x_d + x_s)/2$ with the radius depending on t which is the level surface of the distance function, and we have used this to define the well-separated multiple point targets.

As for much more practical situations, we will consider the following cases in our next FDOT study. They are the cases where the targets are not point targets, and the measurement surface $\partial\Omega$ is curved. The first task to start this study will be to have the Green function for the FDOT under the setup, including these cases. This is available by easily modifying the argument in one of our coauthors' papers [21] giving the Green function for the interior transmission problem. The advantage of the mentioned argument is based on using the parabolic scaling which immediately gives the dominant part of the Green function. In relation to this, we note that the distance function is invariant under the parabolic scaling. Assuming the targets are well-separated convex domains and looking at the dominant part of the Green function, we speculate that we will find a similar situation as for the point target case in a neighborhood of the point that the mentioned sphere touches the target.

Author contributions

Shuli Chen: Formal analysis, Numerical simulation, Writing - original draft; Junyong Eom: Conceptualization, Mathematical analysis, Validation, Writing - original draft; Nakamura Gen: Proposing asymptotic

methods for Section 2, Writing, Editing; Nishimura Goro: Proposing the idea of this study, Physical interpretation of the results, Writing - review and editing. All authors have read and agreed to the published version of the manuscript

References

[1] H. Ammari, J. Garnier, L. Giovangigli, Mathematical modeling of fluorescence diffuse optical imaging of cell membrane potential changes, *Quart. Appl. Math.*, 72 (2014) 137–176.

[2] A. N. Bashkatov, E. A. Genina, V. V. Tuchin, Optical properties of skin, subcutaneous, and muscle tissues: a review, *J. Innov. Opt. Heal. Sci.*, 4 (2011) 9–38.

[3] N. Ducros, C. Andrea, A. Bassi, F. Peyrin, Fluorescence diffuse optical tomography: Time-resolved versus continuous–wave in the reflectance configuration, *IRBM*, 32 (2011) 243–250.

[4] S. Chen, J. Eom, G. Nakamura, G. Nishimura, Approximate peak time and its application to time-domain fluorescence diffuse optical tomography, *Commun. Anal. Comput.*, 1 (2023) 379–406.

[5] J. Eom, M. Machida, G. Nakamura, G. Nishimura, C. Sun, Expressions of the peak time for time-domain boundary measurements of diffuse light, *J. Math. Phys.*, 64 (2023) 083504.

[6] D. Hall, G. Ma, F. Lesage, Y. Wang, Simple time–domain optical method for estimating the depth and concentration of a fluorescent inclusion in a turbid medium, *Opt. Lett.*, 29 (2004) 2258–2260.

[7] S. Han, S. Farshchi-Heydari, D. Hall, Analytical method for the fast time–domain reconstruction of fluorescent inclusions in vitro and in vivo, *Biophys. J.*, 98 (2010) 350–357.

[8] L. Hervé, A. Koenig, J. M. Dinten, Non-uniqueness in fluorescence-enhanced continuous wave diffuse optical tomography, *J. Opt.*, 13 (2011) 015702.

[9] Y. Hoshi, Y. Yamada, Overview of diffuse optical tomography and its clinical applications, *J. Biomed. Opt.*, 9 (2016) 091312.

[10] J. Hebden, R. Kruger, K. Wong, Time resolved imaging through a highly scattering medium, *Appl. Opt.*, 30 (1991) 788–794.

[11] J. Hebden, S. Arridge, D. Deply, Optical imaging in medicine: I. Experimental technique, *Phys. Med. Biol.*, 42 (1997) 825–840.

[12] H. Jiang, *Diffuse optical tomography: principles and applications*, CRC Press, Boca Raton, 2010.

[13] H. Jiang, *Fluorescence Molecular Tomography: Principles and Applications*, Springer, Cham, Switzerland, 2022.

[14] J. R. Lakowicz, *Principles of Fluorescence Spectroscopy*, Second Edition, Kluwer Academic/Plenum Publishers, New York, 1999.

[15] S. Lam, F. Lesage, X. Intes, Time domain fluorescent diffuse optical tomography: analytical expressions, *Opt. Exp.*, 13 (2005) 2263–2275.

[16] J. Liu, M. Machida, G. Nakamura, G. Nishimura, C. Sun, On fluorescence imaging: the diffusion equation model and recovery of the absorption coefficient of fluorophores, *Sci. China Math.*, 65 (2022) 1179–1198.

[17] Y. Liu, W. Ren, H. Ammari, Robust reconstruction of fluorescence molecular tomography with an optimized illumination pattern, *Inverse Probl. Imag.* 14 (2020) 535–568.

[18] A. Milstein, S. Oh, K. Webb, C. Bouman, Q. Zhang, D. Boas, R. Millane, Fluorescence optical diffusion tomography, *Appl. Opt.*, 42 (2003) 3081–3094.

[19] M. Mycek, B. Pogue, *Handbook of Biomedical Fluorescence*, Marcel Dekker, New York, 2003.

[20] V. Nitziachristos, C. Tung, C. Bremer, R. Weissleder, Fluorescence molecular tomography resolves protease activity in vivo, *Nat. Med.*, 8 (2002) 757–761.

[21] G. Nakamura, H. Wang, Solvability of interior transmission problem for the diffusion equation by construting its Green function, *J. Inverse Ill-Pose. Probl.*, 27 (2019) 671–701.

[22] K. Papadimitriou, E. Rosas, E. Zhand, R. Cooper, J. Hebden, S. Arridge, S. Powell, Dual wavelength spread-spectrum time-resolved diffuse optical instrument for the measurement of human brain functional responses, *Biomed. Opt. Express*, 11 (2020) 3477–3490.

[23] K. Prieto, G. Nishimura, A new scheme of the time-domain fluorescence tomography for a semi-infinite turbid medium, *Opt. Rev.*, 24 (2017) 242–251.

[24] G. Nishimura, T. Suzuki, Y. Yamada, H. Niwa, T. Koike, Depth detection limit of a fluorescent object in tissue-like medium with background emission in continuous-wave measurements: a phantom study, *J. Biomed. Opt.*, 29 (2024) 097001.

[25] P. Taroni, A. Pifferi, A. Torricelli, D. Comelli, R. Cubeddu, In vivo absorption and scattering spectroscopy of biological tissues, *Photoch. Photobio. Sci.*, 2 (2023), 124–129.